Importance of the Equatorial Undercurrent on the Sea Surface Salinity in the Eastern Equatorial Atlantic in boreal spring

C. Y. Da-Allada[1], J. Jouanno[2], F. Gaillard[3], N. Kolodziejczyk[4], C. Maes[1], N. Reul[3], and B. Bourlès[5]

Corresponding author[1]: Casimir Y. DA- ALLADA, IRD/Ifremer, Plouzané, France

[1]IRD/LOPS, IFREMER, CNRS, Univ. Brest, IUEM, Brest, France.

[2] LEGOS, Université de Toulouse, CNES, CNRS, IRD, UPS, Toulouse, France

[3]IFREMER/LOPS, CNRS, IRD, Univ. Brest, IUEM, Brest, France.

[4]IUEM/LOPS, IFREMER, CNRS, IRD, Univ. Brest, Brest, France.

[5]IRD/LEGOS, Brest, France

Key points:

Large SSS increase during boreal spring in the equatorial Atlantic Cold Tongue (ACT).

Oceanic vertical processes drive the boreal spring SSS maximum.

Explaining the erosion of the EUC salinity in the ACT with 1-month lag between the maximum of SSS in June and the minimum SST observed in July.

Abstract

The physical processes implied in the sea surface salinity (SSS) increase in the equatorial Atlantic Cold Tongue (ACT) region during boreal spring and the lag observed between boreal spring SSS maximum and sea surface temperature (SST) summer minimum are examined using mixed-layer salinity budgets computed from observations and model during the period 2010-2012. The boreal spring SSS maximum is mainly explained by an upward flux of high salinity originating from the core of the Equatorial Undercurrent (EUC) through vertical mixing and advection. The vertical mixing contribution to the mixed-layer salt budget peaks in April-May. It is controlled primarily by i) an increased zonal shear between the surface South Equatorial Current and the subsurface EUC and ii) the presence of a strong salinity stratification at the mixed-layer base from December to May. This haline stratification that is due to both high precipitations below the Inter Tropical Convergence Zone (that is at its southernmost position during boreal winter and early-spring) and zonal advection of low-salinity water from the Gulf of Guinea, explains largely the seasonal cycle of the vertical advection contribution to the mixed-layer salt budget. In the ACT region, the 1-month lag observed between the maximum of SSS in June and the minimum of SST in July is explained by the shallowing of the EUC salinity core in June, then the weakening/erosion of the EUC in June-July which reduces the lateral subsurface supply of high saline waters.

Keywords: Atlantic cold tongue, SMOS SSS, model, EUC salinity maximum, vertical processes

1. **Introduction**

The eastern equatorial Atlantic Ocean presents a marked seasonal cycle whose main feature is the seasonal formation of the Atlantic Cold Tongue (ACT) during boreal summer [*Chang et al*., 2005; *Peter et al*., 2006; *Giordani and Caniaux*, 2011; *Wade et al*., 2011; *Caniaux et al.*, 2011; *Burmeister et al*., 2016], an area with cool waters extending from the African coast to approximately 20°W, with the lowest temperatures occurring along and south of the equator (Fig. 1a). During boreal spring/summer the southeasterly trade winds intensify [*Hastenrath and Lamb*, 1978; *Philander and Pacanowski*, 1981], pushing the Inter-Tropical Convergence Zone (ITCZ) northward [*Picaut,* 1983; *Waliser and Gautier* 1993] and intensifying the equatorial near surface mixing and upwelling [e.g., *Jouanno et al.*, 2011; *Caniaux et al.*, 2011].

Recent advances have been made in understanding the spatial and temporal variability of the sea surface temperature (SST) in the ACT region. Observations and models highlight the crucial role played by the vertical turbulent mixing between the westward flowing South Equatorial Current (SEC), and the subsurface eastward Equatorial Undercurrent (EUC) in controlling the seasonal formation of the ACT [*Peter et al.*, 2006; *Wade et al*., 2011; *Jouanno et al.,* 2011; *Hummels et al.,* 2013]. It is also expected that these subsurface processes involved in the upper ocean heat balance may have a significant influence on the seasonal variability of the upper ocean salinity and the Sea Surface Salinity (SSS).

Contrary to temperature, only a few studies focused on the ACT salinity variability though it may play an important role on the regional dynamics and air-sea exchanges through its influence on the stratification of the water column and consequently, on the mixed-layer depth (MLD) and large scale density gradients [*Lukas and Lindstrom*, 1991; *Sprintall and Tomczak*, 1992; *Pailler et al*, 1999; *Maes and O'Kane,* 2014]. Changes in SSS are also related to changes in the hydrological cycle [*Webster*, 1994; *Hosoda et al.*, 2009; *Helm et al*., 2010; *Durack and Wijffels*, 2010; *Yu*, 2011; *Terray et al.*, 2012; *Da-Allada et al*., 2014a]. So, a better knowledge of the SSS could provide better estimate of the oceanic freshwater flux and thus, improve our understanding of the variability of the freshwater flux at the ocean surface [e.g., *Ren et al*., 2014].

In the Tropical Atlantic, seasonal SSS variations are controlled by different processes depending on the region considered. For instance, studies on the mixed-layer salinity budget estimated from observations and ocean circulation models indicate that the SSS seasonal variability in the western tropical North Atlantic is mainly due to horizontal salinity advection [e.g., *Foltz et al.*, 2004; *Foltz and McPhaden*, 2008; *Da-Allada et al*., 2013] and large river discharges [*Reul et al*., 2014a; 2014b] while in the central and eastern tropical North Atlantic, the seasonal cycle of the precipitations plays a major role on the SSS seasonal cycle [*Foltz et al.*, 2004; *Foltz and McPhaden*, 2008; *Tzortzi et al.*, 2013; *Da-Allada et al*., 2013; 2014b]. In the Gulf of Guinea, contributions of the vertical mixing and vertical salinity advection on the salt budget explain the seasonal variability of the SSS [*Tzortzi et al.*, 2013; *Da-Allada et al*., 2013; 2014b; *Berger et al.*, 2014; *Camara et al*., 2015]. The recent numerical study by *Camara et al*. [2015] in the central equatorial Atlantic also underlined the important role of the vertical mixing in the seasonal cycle of the SSS.

In the ACT region, based on combined in situ observations collected from May to July 2011 during the Cold Tongue Experiment (CTE), model, reanalysis, and satellite data, *Schlundt et al.* [2014] investigated the mechanisms responsible for the SSS variability during the development of the ACT. They mainly focused on two regions: the western equatorial ACT (23°-10°W) and the region north of the ACT. They found that in the region north of the ACT, salinity variability is mainly due to precipitation and zonal advection, whereas in the western equatorial ACT region, evaporation and the zonal advection drive the SSS variations. Although the salinity tendency variations diagnosed in the north of ACT matched the observed ones within error bars, *Schlundt et al.* [2014] found large discrepancies in the western ACT region during May, and they suggested that the advection term may be underestimated because of horizontal salinity gradients not properly resolved in their dataset. At Equator-10°W, their analysis also showed a strong SSS increase in boreal spring lagged by the SST cooling of about one month. However, no physical processes was proposed or described to explain these timing.

Progress have been recently made in SSS observation thanks to the new Satellite SSS measurements provided by the European Space Agency Soil Moisture and Ocean Salinity (ESA/SMOS) [*Reul et al.*, 2012] or by the Aquarius/SACD mission [*Lagerloef*, 2012] that are available from 2010-present and 2011-2015, respectively. Satellite measurements offer the opportunity to observe the SSS with an unprecedented resolution (50-100 km/3 days) and with an accuracy of 0.4 PSS (Practical Salinity Scale, according to the 1978 practical salinity scale) in the Tropical regions [*Lee et al*., 2012; 2014; *Hernandez et al.,* 2014; *Reul et al.,* 2014a, 2014b; *Lu et al*, 2016]. In the tropical Atlantic, satellite observations allow to monitor the seasonal SSS variability [*Tzortzi et al.,* 2013] and to detect tropical instability waves (TIWs) [*Lee et al.,* 2014]. *Lee et al.* [2014] showed that SSS horizontal gradient significantly contributes to the dynamical balance of TIWs by enhancing the meridional density gradient in the tropical Atlantic, especially during boreal spring.

Up to now, the main processes which drive the seasonal variability of the SSS in the ACT region have not been fully understood and no explanation has been proposed for boreal spring SSS maximum as mentioned first by *Schlundt et al.* [2014]. This study addresses the following questions: i) What are the surface and subsurface processes driving the SSS seasonal variability in the ACT? and, ii) What explains the lag between SST summer minimum and boreal spring SSS maximum?

The remainder of this paper is organized as follows. Section 2 presents the methodology, observations data, the model description and validation. In Section 3, the SSS seasonal variability is investigated, with a focus on SSS boreal spring maximum and phasing. Discussion and conclusions are given in Section 4.

2. Methods, data and Model

2.1 The mixed-layer salt budget

The mechanisms controlling the seasonal variability of the SSS in the ACT are investigated by analyzing the mixed-layer salinity budget which reads [*Foltz and McPhaden*, 2008; *Qu et al*., 2011; *Da-Allada et al*., 2013; 2015; *Schlundt et al.*, 2014]:

$$\frac{\partial SSS}{\partial t} = \underbrace{\frac{(E-P-R)SSS}{h}}_{FLX} \underbrace{\underbrace{-\langle u.\partial_x S\rangle}_{XAD} \underbrace{-\langle v.\partial_y S\rangle}_{YAD}}_{HAD} \underbrace{\underbrace{-\langle w.\partial_z S\rangle}_{ZAD} \underbrace{-\frac{(k_z \partial_z S)_{z=-h}}{h}}_{ZDF} \underbrace{-\frac{1}{h}\frac{\partial h}{\partial t}(SSS - S_{z=-h})}_{ENT}}_{VPR} \underbrace{+D_l(S)}_{LDF} \quad (Eq.1)$$

with $\langle \bullet \rangle = \frac{1}{h}\int \bullet \, d_Z \quad (Eq.2)$

S the salinity averaged within the mixed-layer, E the evaporation, P the precipitation, R the river runoffs, h the depth of the mixed-layer, (u, v, w) the zonal, meridional and vertical components of the velocity vector, k_z the vertical diffusion coefficient and $D_l(S)$ the lateral diffusion contribution.

The left-hand side (lhs) term of Eq.1 represents the mixed-layer salinity tendency. At the right-hand side (rhs) of Eq.1, the term FLX is the surface freshwater flux, XAD is the zonal salinity advection, YAD is the meridional salinity advection, ZAD is the vertical salinity advection, ZDF represents the vertical diffusion at the base of the mixed-layer, ENT is the entrainment at the base of the mixed-layer, and the term LDF is the lateral diffusion.

The sum of XAD and YAD represents the horizontal salinity advection (HAD). In the following, the vertical processes are combined under the term VPR (VPR=ZAD+ZDF+ENT). In this study, we analyze and compare the SSS budget calculated both from observations and model outputs. Since SMOS data are limited to the surface [e.g., *Boutin et al*. 2016], the VPR contribution in the observations is estimated as the difference between the SSS tendency and the sum of FLX, HAD and LDF. So, this term could also contain sampling and observations errors. The horizontal diffusion contribution to the salinity budget is computed using a Laplacian operator with a diffusion coefficient set to 500 m^2 s^{-1} in the observations (as in *Dong et al*. [2009], *Yu* [2011] or *Da-Allada et al* [2015]) and set to 300 m^2 s^{-1} in the model.

The error bar (e) for the observed SSS tendency in the Eq.1 is calculated following the formulation used in several studies [e.g. *Foltz and McPhaden,* 2008; *Da-Allada et al.*, 2015; *Camara et al.*, 2015] : $e = \left(\sqrt{e_{S_{t+1}}^2 + e_{S_{t-1}}^2}\right) / \Delta t$, with Δt = 2 months and e_S is the SSS error given by the standard error of all available SSS data for each month of the study period.

The river runoff term, R, will not be included in our estimates since we focus on regions sufficiently far away from the coast and not under the influence of either Congo or Niger River plumes [e.g. see Figure 10 in *Reul et al.*, 2014b].

2.2 Observations data

The surface salinity data used in this study to evaluate the SSS budget terms from observations are derived from the SMOS satellite data, a mission that has been launched on November 2nd, 2009. In the present study, we use the so-called SMOS Level 4a SSS products provided by the Centre Aval de Traitement des Données SMOS (CATDS, http://www.catds.fr/), and referred to as the IFREMER Expertise Center-Ocean Salinity (CEC-OS) products. These datasets are weekly composite at a spatial resolution of 0.5°×0.5° and are available for the 2010-2014 period. These new products are computed like the Level 3 products [*Reul and Tenerelli,* 2011] except that the large scale bias corrections that are applied to the swath products consider the monthly climatology of the SSS obtained from the In Situ Analysis System (ISAS) SSS [*Gaillard et al*., 2016] instead of the fields from the World Ocean Atlas (2001) [*Conkright et al.*, 2002].

We used the 1/3° resolution surface current products with a 5-day temporal resolution from Ocean Surface Current Analyses Realtime (OSCAR) [*Lagerlof et al.*, 1999; *Bonjean and Lagerlof*, 2002] (http://www.oscar.noaa.gov/), directly calculated from satellite altimetry and ocean vector winds.

For characterizing the MLD, we use a monthly seasonal cycle of the MLD (defined as the depth where the density is 0.03 $kg.m^{-3}$ greater than the 10 m depth density) from the climatology of de *Boyer Montégut et al.* [2004] available on a 2°×2° grid and derived from World Ocean Circulation Experiment (WOCE) and the National Oceanographic Data Center (NODC).

Monthly evaporation and precipitations are from the ERA-Interim reanalysis [*Dee et al*., 2011] of the European Centre for Medium-Range Weather Forecasts (ECMWF) and are available monthly from 1979 up to present with a 0.5° resolution.

2.3 Ancillary data

The model SST is compared with satellite SST data provided by the TRMM (Tropical Rainfall Measuring Mission) Microwave Imager (TMI) [*Kummerow et al*., 1998]. The SST data are available from 1998 with a 1/4° horizontal resolution. Monthly salinity and temperature measurements from the PIRATA mooring located at 10°W, 0° [*Bourlès et al*., 2008] are used to observe the seasonal variations of the salinity core of the EUC. This mooring provides salinity measurements at 6 vertical levels from the surface (1 m depth) down to 120 m depth with a 20 m resolution, while temperature is measured at 11 vertical levels between 1 and 500 m depth with 20 m resolution in the upper 140 m. These data are available from 1997 up to present.

2.4 OGCM

A regional numerical simulation of the Tropical Atlantic based on NEMO3.6 (Nucleus for European Modeling of the Ocean, *Madec*, 2014) is analyzed in this study. The numerical setup is fully described in *Hernandez et al*. [2016], together with some comparisons with observations. The regional configuration extends from 35°S to 35°N and from 100°W to 15°E with a quarter degree horizontal resolution. The model solves the three dimensional primitive equations discretized on an Arakawa C grid at fixed vertical levels and has 75 vertical levels (12 levels within the first 20 m and 24 levels in the upper 100 m). The momentum advection is based on the 3rd order upstream biased scheme which includes an implicit diffusion. Tracer advection is performed using a Total Variance Dissipation (TVD) scheme and tracer diffusion is parameterized with a Laplacian isopycnal operator with a coefficient of 300 m^2 s^{-1}. The vertical diffusion coefficient is given by a GLS (Generic Length Scale) scheme with a k-ε turbulent closure [*Umlauf and Burchard*, 2003, *Reffray et al.* 2015].

The model is forced at the lateral boundaries with daily outputs of the global MERCATOR reanalysis GLORYS2V3. At the surface, the atmospheric fluxes of momentum, heat and freshwater are computed using bulk formulation [*Large and Yeager*, 2004] and the DRAKKAR Forcing Set 5.2 (DFS5.2) product [*Dussin et al*., 2014]. DFS5.2 is derived from ERA-Interim reanalysis (3-h fields of wind speed, atmospheric temperature and humidity, and daily fields for long and short wave radiation and precipitation) from ECMWF [*Dee et al.*, 2011]. River runoffs are prescribed near the river mouths as a surface freshwater flux using the monthly climatology of *Dai and Trenberth* [2002].

The model is initialized at day January 1st, 1979 using salinity and temperature derived from the Levitus climatology and is integrated over the period 1979-2012. There is no surface salinity restoring toward a climatological SSS. Each terms of the Eq.1 except the entrainment term, which is deducted as a residual, are computed at each model time step. In this study, we used monthly averages of the mixed-layer trends, as in *Da-Allada et al*. [2014b] or *Camara et al*. [2015].

In order to further investigate the subsurface processes that may be involved in the mixed-layer budget, we also computed and analyzed the different contributions to the model 3-dimensional salinity balance:

$$\partial_t S = \underbrace{-u.\partial_x S - v.\partial_y S - w.\partial_z S}_{ADV} \quad \underbrace{-\partial_z (K_z \partial_z S)}_{ZDF} \quad + LDF(S) + FOR(z) \quad (Eq.3)$$

where S is the model salinity, ADV is the 3d salinity advection, ZDF is the vertical diffusion, LDF is the horizontal diffusion, FOR is the tendency of salinity due to E-P-R at the surface.

The vertical turbulent salt flux (TSF_{ZDF}) is calculated at different depths z as follows:

$$TSF_{ZDF} = \int_{-z}^{0} \partial_Z (K_z \partial_z S) dz \quad (Eq.4)$$

and assuming that there is no diffusive fluxes at the surface.

The density stratification [*Maes and O'Kane*, 2014] is described by the Brunt-Väisälä frequency $(N^2(T,S))$ determined using the vertical profiles of temperature and salinity as follows: $N^2(T,S) = -\frac{g}{\rho}\frac{\partial \rho}{\partial z} \approx \left(\underbrace{g\alpha \frac{\partial T}{\partial z}}_{N^2(T)} \underbrace{- g\beta \frac{\partial S}{\partial z}}_{N^2(S)} \right) \quad (Eq.5)$

where α is the thermal expansion coefficient, β is the haline contraction coefficient, g is the gravity and ρ is the density. $N^2(T)$ and $N^2(S)$ are the contributions of the temperature and the salinity into the vertical stratification, respectively. The $N^2(T,S)$ estimated above is used with the vertical shear squared (Sh^2) to calculate the non-dimensional Richardson number (R_i) which can be expressed: $R_i = \dfrac{N^2}{Sh^2}$ $(Eq.6)$

where $Sh^2 = \underbrace{\left(\dfrac{\partial u}{\partial z}\right)^2}_{Sh_u{}^2} + \underbrace{\left(\dfrac{\partial v}{\partial z}\right)^2}_{Sh_v{}^2}$ with $Sh_u{}^2$ and $Sh_v{}^2$ the contribution of the vertical shear associated with the zonal and meridional currents, respectively.

Finally, a mean salinity budget within the EUC is performed. This salinity budget is calculated by integrating vertically the dominant salinity balance (Eq.3) between the two isopycnals that define the salinity maximum associated with the EUC in the ACT throughout the year, i.e., between $\sigma_\theta = 24.7\,(z_1)$ and $\sigma_\theta = 26\,(z_2)$ kg.m^{-3}:

$$\partial SF/\partial t = \frac{1}{\Delta z}\int_{-z_2}^{-z_1}(\partial_t S)dz;\ \ XSF = \frac{1}{\Delta z}\int_{-z_2}^{-z_1}(-u.\partial_x S)dz;\ YSF = \frac{1}{\Delta z}\int_{-z_2}^{-z_1}(-v.\partial_y S)dz;\ ZSF = \frac{1}{\Delta z}\int_{-z_2}^{-z_1}(-w.\partial_z S)dz;$$

and $TSF = \dfrac{1}{\Delta z}\displaystyle\int_{-z_2}^{z_1} -\partial_Z\,(K_z \partial_z S)dz;\ with\ \Delta z = z_2 - z_1$ $\left(Eq.7\right)$.

$\partial SF/\partial t$ is the salt tendency, XSF represents the zonal salt advection, YSF is the meridional salt advection, ZSF is the vertical salt advection and TSF is the vertical turbulent salt diffusion. For this balance, we consider neither the lateral diffusion and the entrainment contributions, which were found to be negligible, nor the air-sea freshwater exchanges and runoff, which are limited to the surface and do not affect the isopycnal range we consider for the integration.

A large part of the model analysis is restricted to the period 2010-2012, which is an overlapping period for both model and observations data sets. As the seasonal cycle could be biased due to the short study period, model analysis in the mixed-layer has also been performed over a longer period (1990-2012) in order to verify the robustness of the results obtained (see the discussion section).

2.5 Seasonal variability of SSS and SST

First, we focus on the equatorial ACT region as defined by the box between 3°S-1°N and 17°W-0°E, which is centered on the area with maximum cooling around 1°S-10°W (Fig. 1a) [*Jouanno et al.*, 2011]. The seasonal evolutions of the SSS and SST obtained from observations (SMOS and TMI) in the ACT both present a large seasonal variability (Fig. 1b). The SST exhibits maximum values in the ACT in March/April (SST > 28 °C) and minimum values in July/August (SST < 24 °C). A large SSS increase occurs from April to June (first SSS maximum) followed by a slight SSS decrease period (July/August). Then, the SSS increases again and reaches its second maximum in October/November before decreasing. As already noticed by *Schlundt et al.* [2014], the SSS reaches its maximum in June in the ACT, i.e. one month before the minimum of SST that occurs in July/August.

The seasonal cycle of SSS and SST from the model and observation are compared in Fig. 1b. Throughout the year, the model is saltier than the observation. From January to April, a bias of about 0.5 PSS is observed, which is reduced to about 0.2 PSS from May to December. For the SST, we observe the same seasonality of the bias: a cool bias is observed in the model from December to July (up to -1.5 °C in May-April) while from May to November the bias is weaker. This bias may have multiple origins, including forcing uncertainties or lack of realism of the vertical mixing parameterization. Despite these caveats in the model outputs, the seasonal evolution of the observed SSS and SST are well simulated by the OGCM, with 0.94 and 0.95 correlation coefficients at the 99 % significance level, respectively. Both model and observations exhibit SST maximum in March and minimum SST in July. The two SSS maxima observed in June and in October are also reasonably reproduced in the model.

To further validate the simulated seasonal variability of the vertical distribution of temperature and salinity, in situ salinity and temperature measurements from the PIRATA mooring located at 10°W-0°N are compared with the model. Although the model salinity is larger than the PIRATA data, the simulated seasonal variability of the salinity vertical structure is in phase with observed cycle (Fig. 2). Near the surface (0-30 m), model and observations both exhibit two salinity maxima previously observed in the seasonal cycle of SMOS SSS. At subsurface (below 30 m), both model and observations present a pronounced subsurface salinity maximum, associated with the EUC between 40 and 80 m, which follows a semi-annual cycle. The seasonal cycle and distribution of the model temperature at 10°W-0°N is also in good agreement with the PIRATA data (Fig. 3): i) the formation of the cold tongue in the model is in phase with the observations and ii) the position of the depth of the isotherm 20 °C, a representative proxy for the thermocline depth, is also qualitatively comparable in the model and the observations. Overall, these validations give us confidence on the capability of the simulation to reproduce the observed variability at seasonal time scales in the ACT region.

3 Results

3.1 Boreal spring SSS maximum in the ACT region

In order to explain the boreal spring SSS increase, the contributions to the mixed-layer salinity balance in the ACT region are examined using mixed-layer salinity balances computed both from the observations and from the model (Fig. 4). The SSS tendencies obtained from the observations and from the model show similar seasonal cycles (0.83 correlation coefficient at the 99 % significance level). Both tendencies exhibit two salinization events during the year: the largest in May (+0.40 PSS. month^{-1}) and a secondary maximum in September (+0.12 PSS. month^{-1}). The spring salinization starts one month later in the model compared to the observations. Despite small differences between the model and observations, all terms in the rhs of Eq.1 are in phase and present very similar seasonal cycles

(Fig. 4b). The contributions of the ocean vertical processes (VPR) and of the horizontal advection (HAD) present a larger seasonal cycle than the surface freshwater flux (FLX). The VPR is positive throughout the year and leads to an important increase in SSS from December to June. Its contribution is strongly reduced during the rest of the year (July to November). The first strongest SSS increase in May is clearly attributed to the vertical processes. The horizontal SSS advection is dominated by the zonal advection (Fig. 5a). Both are negative all year long due to the westward transport of low-salinity water from the Gulf of Guinea by the SEC (Fig. 4b and Fig. 5a) [*Schlundt et al.*,2014; *Da-Allada et al.*, 2014b; *Camara et al.*, 2015]. The HAD is responsible for the large SSS decrease observed in December both in the model and observations. The HAD contributes significantly to the SSS budget at the exception of the September/October period when this term is almost negligible. The FLX is negative from December to April when the ITCZ is located near the equator and therefore contributes to reduce the SSS in the ACT during this period. During the rest of the year (from May to November), the FLX is dominated by evaporation and acts to increase the SSS, summing to the VPR. During September-October, the contributions of the HAD and of the VPR to the mixed-layer salinity budget are weak, so the FLX is the main contributor to the surface salinization observed during this period.

3.1.1 Vertical processes

As detailed above, the contribution of the VPR in the salt budget obtained from observations is estimated as a residual of Eq. 3. The seasonal cycle of the observed VPR contribution is in agreement with that of the model with a maximum in April and a minimum in October (Fig. 4b). Consequently, we consider that the model is suitable to explore in details the vertical processes that are inaccessible from any other means (neither in situ measurements, nor satellite missions).

To a first order, the VPR contribution to the mixed-layer salt budget is explained by co-varying vertical advection and diffusion (Fig. 5b). These two terms are of same order of magnitude and vary in phase during the seasonal cycle. Analyzing the 3D salinity budget (see Eq.3), we find that the vertical diffusion acts to increase the salinity in the mixed-layer throughout the year (Fig. 6a), consistently with the positive ZDF trend for the mixed-layer salt budget (Fig. 5b). ZDF exhibits peaks in April/May and December/January, period which also coincides with the strongest vertical turbulent salt flux TSF (Fig. 6b). The high values of vertical turbulent salt flux occur in the 10-30 meters depth range, which correspond to a depth range with low Richardson number (Fig. 6b) and large vertical shear (Fig. 6c-d). Note that the zonal velocity shear controls the total horizontal shear (Fig. 6c-d). The vertical shear peaks near 20 m and its seasonal variability is driven by the strength of the surface SEC (Fig. 6c-d and Fig. 7a-b). Note that there is no direct link between the seasonal variability of the local wind stress (Fig 7e) and the turbulent fluxes of salt, suggesting that the local wind forcing does not control the turbulent fluxes of salt (at the difference of the basin scale wind variability that drives the SEC and indirectly modulates the vertical shear of the equatorial currents).

As for the vertical diffusion, the vertical salinity advection contributes to increase the mixed-layer salinity throughout the year with an important contribution from December to May (Fig. 5b). This term, which is a function of both the vertical salinity gradient and the vertical velocity, brings salty water from the subsurface EUC up to the mixed-layer. To first order, the seasonal evolution of the vertical advection contribution to the mixed-layer balance is in phase with the variability of the salinity vertical gradients at the mixed-layer base but not with the seasonal cycle of the vertical velocity (upward throughout the year) that peaks in May and November (Fig. 7c-d). This suggests that the variability of vertical salinity advection is mainly explained by the strong salinity stratification variability at the base of the mixed-layer (Fig. 7c), except in May, when vertical salinity advection is reinforced by the strong upward velocity (Fig. 7d). The strong salinity stratification observed from December to May is due to the zonal advection of surface freshwater and precipitation (Fig. 4b and Fig. 5a). The maximum upward vertical velocity that corresponds to the equatorial upwelling is observed when the wind stress is at its maximum (Fig. 7e). The intensification of trade winds in the equatorial region generates upwelling equatorial Kelvin waves that are responsible for the shoaling of the thermocline observed in May-June (Fig. 7c). Note that the thermocline shoaling could also contribute to enhance the vertical salinity gradient at the MLD base.

3.2 Lag between SSS maximum and SST minimum: role of the EUC salinity maximum

As previously shown, the vertical mixing between the SEC and the upper part of the EUC mainly explains the seasonal ACT surface salinization. Although similar mechanisms are involved in the equatorial seasonal cooling and associated ACT formation [e.g., *Peter et al.* 2006, *Jouanno et al.* 2011], there is an intriguing 1-month lag between the SSS maximum and the SST minimum (Fig. 1b). It would be interesting to understand this difference in the seasonal cycle.

The vertical structures of the salinity and the temperature averaged in the ACT region present similar seasonal evolutions to that inferred at 10°W, 0°E at the surface (Fig. 2 and Fig. 3) but with differences at the subsurface (Fig. 8). Subsurface salinity maximum associated with the EUC is between 40 and 60 m in the ACT instead of 40-80 m at 10°W-0°N and there is also a more intense cooling at 10°W-0°N than in the ACT. The SSS maximum observed in June (Fig. 8a) appears one month before the July SST minimum (Fig. 8b) as in PIRATA observations (Fig. 2a and Fig. 3a). The salinity maximum associated with the EUC is located throughout the year between $\sigma_\theta = 24.7\ kg.m^{-3}$ and $\sigma_\theta = 26\ kg.m^{-3}$ and shows a semi-annual cycle, with peaks in March/April and November (Fig. 8a). During boreal spring, the salinity maximum enters the mixed-layer, and is then totally eroded in early boreal summer. On the other hand, because of continuous positive vertical temperature gradient in the upper ocean, input of cool water from subsurface is sustained during boreal summer while the maximum SSS disappears (due to zonal advection of freshwater in the mixed-layer, Fig. 5a). Due to the erosion of the EUC salinity core in early boreal summer, the vertical salt flux induced by the subsurface processes is strongly reduced in July while SST cooling is sustained.

To explore why the EUC salinity maximum is eroded during boreal summer, we analyze the salinity and velocity averaged between the two aforementioned isopycnals ($\sigma_\theta = 24.7\ kg.m^{-3}$ and $\sigma_\theta = 26\ kg.m^{-3}$), representative of the EUC core. First, we find that the erosion of the salinity maximum at the equator is not due to the meridional displacement of the core of the EUC (Fig. 9a). Moreover, the semi-annual cycle of the salinity along the equator is consistently observed from the African coast to 30°W (Fig 10). This semi-annual cycle of the EUC salinity (Fig. 9a) follows that of the EUC zonal speed (Fig. 9b) with 1-month lag, suggesting a close link between the EUC intensity and its haline content. During boreal summer, the EUC is weak and thus the salt transport by the EUC is reduced, suggesting that the boreal summer erosion of the EUC maximum salinity could be due to the weakening of the EUC. It is also likely that the meridional current exports high salinity waters southward and importing low salinity waters from the north (Fig. 9c and Fig. 10). Note that the seasonal cycle of the vertical diffusion is negative throughout the year between the 24.7 and 26 isopycnals so this process also contributes to the erosion of the high salinity core of the EUC all along the year with maximum during the April to July period (Fig. 6a).

In order to quantify the respective role of advection and vertical diffusion processes on the erosion of the EUC high salinity core in boreal summer, the seasonal EUC salinity budget (averaged within the ACT and between the 24,7 and 26 kg.m^{-3} isopycnals; Eq.7) is analyzed. In agreement with the previously discussed salinity seasonal cycle within the EUC (Fig. 9a), the seasonal cycle of the salt tendency is negative from April to August and in November and positive the rest of the year with a maximum in September (Fig. 11). The zonal salt advection (XSF) exhibits a similar seasonal evolution suggesting that it is the major driver of the decrease of the EUC salinity maximum. The vertical turbulent salt flux (TSF) driven by the vertical shear permanently contributes to erode the EUC salinity maximum (Fig. 6a, c and Fig. 11). The negative salt tendency observed in May is due to the maximum effect (-0.18 PSS.month^{-1}) of the TSF. The meridional salt advection (YSF) exhibits a strong seasonal cycle and is maximum in July (> -0.21 PSS.month^{-1}), due to the intensification of the meridional current in the EUC (Fig. 9c and Fig. 11). The seasonal evolution of the vertical salt advection (ZSF) is similar to the meridional salt advection one (Fig. 11). ZSF tends to increase salinity in order to compensate its decrease due to the meridional salt flux. The contribution of the vertical advection shows an important increase in May (+0.24 PSS.month^{-1}) and July (> +0.27 PSS.month^{-1}) that is due to the maximum vertical velocity in the EUC (Fig. 7d and Fig. 11).

4 Discussion and Conclusion

The recent high resolution SMOS salinity data obtained from the CATDS/SMOS reveal an important seasonal SSS variability in the ACT region with two salinization events during the year: the first and largest SSS increase appears in boreal spring and the second, smaller, in September/October. In this ACT region, a 1-month lag is also observed between the maximum of SSS in June and the minimum of SST in July. As the eastern equatorial Atlantic Ocean is known to be associated with intense seasonal variability of the SST, it is important to elucidate the details at work in this interplay.

This paper investigates the physical processes that are responsible for the boreal spring SSS increase and for the observed lag between the SSS maximum and the SST minimum in the ACT region. SMOS salinity data are analyzed, together with a regional numerical simulation of the Tropical Atlantic Ocean. Simulated salinity and temperature are compared with satellite products (SMOS and TMI) and with PIRATA mooring measurements located at 10°W-0°N. Although a salt bias exists between the model and the observations, the model reproduces consistently the observed seasonal cycles of the salinity and temperature in the region. This allows us to use both model and observations with confidence to diagnose the dominant physical mechanisms at work.

The boreal spring SSS maximum in the ACT is due to subsurface processes that bring salty waters in the mixed-layer, while from September-October, the local evaporation is the main contributor to the SSS increase. Vertical mixing and vertical advection are found to have similar contributions to the salt input into the mixed-layer, with vertical mixing variability well explained by the zonal shear variability between the surface SEC and subsurface EUC. Although the importance of the vertical velocity in the eastern equatorial Atlantic has already been noted during this year period by several studies [e.g., *Rhein et al.*, 2010; *Giordani and Caniaux*, 2011], we find that the seasonal cycle of the vertical velocity does not control the vertical advection at first order. Instead, the seasonal variability of the vertical advection of salt in the mixed-layer is largely explained by the seasonal variability of the salinity stratification observed at the MLD base. For the rest of SSS balance terms, the horizontal advection contributes permanently to decrease the SSS in the ACT region. This contribution is mainly due to zonal advection by the SEC of low-salinity water from the Gulf of Guinea to the ACT region. From December to April, when the ITCZ is close to the equator, the surface freshwater flux acts to decrease the SSS while the rest of the year, evaporation dominates in the ACT and increases the SSS.

Although our study region differs slightly from *Schlundt et al*. [2014] and *Camara et al.* [2015], our SSS balance analysis also suggests that the vertical processes play a crucial role in the SSS variability. As reported by *Schlundt et al*., [2014], the vertical mixing was estimated using micro-structure profiles obtained between May and July. That is why *Schlundt et al*. [2014] missed the physical processes responsible for the increase in SSS before the ACT set up. This is also likely the reason why they also missed the strong positive contribution of the vertical mixing from December to May. In contrast, in agreement with the present study, *Camara et al.*, [2015] found that the vertical mixing driven by the vertical shear has an important contribution for the SSS budget. As the vertical mixing is parameterized in the model, it would be interesting in the future to make micro-structure measurements earlier in boreal spring to better explore and document the mixing conditions in the upper ocean layers of this region.

During the SSS increase, both studies reported by *Schlundt et al*. [2014] and by *Camara et al.*, [2015] found that the vertical salinity advection term is negligible, while in our model the vertical advection presents a contribution similar to the vertical mixing. This term is included in the entrainment term in the study by *Schlundt et al*. [2014] and depends on the MLD, the vertical velocity and the vertical salinity gradient at the base of the mixed-layer. *Schlundt et al*. [2014] used a temperature criterion to define the MLD while a density criterion is used in our study. We found that the contribution of the vertical advection to the mixed-layer salt balance in the ACT is largely due to the seasonal variability of the salinity stratification at the mixed-layer. Thus, the difference between our result and their estimate of the vertical advection term is likely explained by their MLD criteria or the lower vertical resolution of the in-situ data that may not allow to properly estimate the vertical salinity gradient at the mixed-layer base. As a consequence, the present study suggests that the residual term diagnosed by *Schlundt et al*. [2014] study may not only be explained by the lack of resolution in the zonal and meridional salinity gradients, but also by the vertical processes which are hardly accessible with observations. Using another OGCM model, *Camara et al.*, [2015] choose a different density criterion for the MLD (0.01 kg.m^{-3} in their study vs 0.03 kg.m^{-3} in our study). They also used a relaxation term toward the observed SSS climatology that could reduce the salinity gradients and thus may explain the weak contribution of the vertical advection they found. As mentioned above, our model has 75 vertical levels vs. 46 in the study of *Camara et al.*, [2015]. Note that the model forcing is also slightly different in the two studies (DFS5.2 in the present study and DFS4 in their study) and may also contribute to the difference in the vertical advection contribution. Thus, it is highly probable that the vertical salinity gradients are better captured in our model and this is a very interesting perspective to keep in mind for further investigations.

In the present study, the seasonal cycle is computed over the longest available overlapping period of observations and simulation (2010-2012). In order to verify the robustness of the present results, the mean seasonal cycle has also been computed from model outputs over a longer period (1990-2012). The results are nevertheless similar to those obtained with the short period (not shown). The dominant terms into the SSS budget that drive the SSS variability remain unchanged although the seasonal evolution of each term of the salinity balance can be slightly shifted. For example, the vertical processes term is maximum in April from our 2010-2012 experiment, while for the period 1990-2012, this term is maximum in May. However, regardless of the time period considered, the SSS tendency reaches its maximum in May. The shift observed in the vertical processes term between the two periods could be explained by the strong interannual variability observed in the equatorial ACT [*Marin et al.*, 2009; *Caniaux et al.*, 2011]. Due to the uncertainties on our present knowledge of interannual to decadal timescales variability in SSS [*O'Kane et al.*, 2016], further investigations are clearly needed to explore the interplay of the seasonal cycle over longer periods of time.

The second important point raised by the present study is the identification of the mechanism explaining the 1-month lag between the maximum SSS observed in June and the minimum SST observed in July in the ACT. The mechanism explaining the phase shift is related to the erosion of the EUC salinity core located throughout the year between $\sigma_\theta = 24.7\ kg.m^{-3}$ and $\sigma_\theta = 26\ kg.m^{-3}$. The upper EUC erosion leads to the disappearance of its associated salinity maximum from July to September, reducing the contribution of vertical mixing and advective salinity flux into the mixed-layer. This happens despite intensified wind stress in July and still high vertical shears at the mixed-layer base in July-August. Therefore, the SSS starts to decrease in June-July, while the upward cooling flux remains intense up to July owing to the vertical distribution of temperature against salinity. This erosion of the equatorial salinity maximum during boreal summer was also reported by several authors based on observations and models [*Gouriou and Reverdin*, 1992; *Kolodziejczyk et al., 2009; 2014; Johns et al.*, 2014].

To understand the disappearance of the EUC salinity maximum during the boreal summer, a seasonal salinity budget of the EUC in the ACT has been analyzed. We find that the major reason for the EUC salinity maximum erosion in July and August is due to the weakening of the zonal salt advection which is mainly related to the weakening of the EUC [*Kolodziejczyk et al., 2009; 2014; Johns et al.*, 2014]. The vertical turbulent salt driven by the vertical shear between the surface and the upper thermocline currents is negative throughout the year and also contributes to decrease the salinity of the EUC. This vertical turbulent salt along with the meridional salt advection tend to compensate the vertical salt advection, except in May and July when the contributions of these terms into the salinity balance are the most important. The strong positive vertical salt advection observed in May and July in the EUC is related to the maximum vertical velocity. These strong values of the vertical velocity inside the ACT were also found at 15°W-0°N in the upper thermocline (~ between 40 and 75 m) in May and July by *Jouanno et al.* [2011]. In boreal summer, due to the intensification of the meridional current in the EUC, the maximum negative meridional salt advection is found in July. This intensification of the equatorial meridional current in boreal summer, when the cold tongue is pronounced, were also observed by *Perez et al.*, [2014] at 10°W. Using observations (moored and shipboard velocity measurements), this latter study characterized the tropical cells as a dominant meridional circulation features in the shallower 100 meters. Thus, the meridional salt advection in July is associated with this circulation pattern, and extends to the salinity field the hypothesis formulated by *Rhein et al.* [2010] that an important meridional heat flux would be associated with the meridional cells in the ACT.

Johns et al. [2014] suggested that the EUC salinity maximum erosion in boreal summer is due to strong mixing that occurs at the top of EUC during the upwelling season. A similar result was found in the eastern part of the basin by *Kolodziejczyk et al*. [2014]. Based on a seasonal box-averaged salinity budget in the upper thermocline delimited by $\sigma_\theta = 24.5\, kg.m^{-3}$ and $\sigma_\theta = 26.2\, kg.m^{-3}$ isopycnals in the eastern Gulf of Guinea (east of 4 ° W), these authors also suggested that the main cause of the equatorial EUC salinity core erosion is due to the intense vertical mixing during the boreal summer although the role of horizontal advection cannot be neglected. In their study, the vertical mixing term was determined as a residual of the salinity budget. In the present study, all terms of the salinity balance in the

EUC could be evaluated. We found that, although the vertical mixing contributes to the erosion of the EUC salinity maximum in the ACT all along the year, this term is not the main cause of this erosion. The major cause of this erosion is related to the weakening of EUC during the boreal summer, which induces a significant diminution of the salt input in the ACT. Overall, this study reveals that the equatorial salinity maximum associated with the EUC plays an important role for the seasonal variability of the SSS.

Acknowledgments

This study benefited from several data sets made freely available : SMOS/ CEC-OS salinity data (www.catds.fr), Ocean Surface Current Analyses-Real time (ftp://podaac-ftp.jpl.nasa.gov/allData/oscar/preview/L4/oscar_third_deg/), ERA Interim reanalysis products provided by European Center for Medium-Range Weather Forecasts (http://data-portal.ecmwf.int/data/d/interim_mnth/), PIRATA mooring data (http://www.pmel.noaa.gov/tao/disdel/disdel.html), TMI data produced by Remote Sensing Systems and sponsored by the NASA (www.remss.com) and the seasonal climatology of the MLD (http://www.ifremer.fr/cerweb/deboyer/mld/Surface_Mixed_Depth.php). The model simulations have been performed on Curie with the GENCI allocation GEN7298. Special thanks are due to Dr Yves du Penhoat (IRD/IRHOB/CIPMA) and Dr Zacharie Sohou (LHMC/IRHOB/CBRST) for the interesting discussions. C.Y. Da-Allada thanks CNES-TOSCA project SMOS and IRD for their support through post-doctoral grants.

References

Berger, H., A. Tréguier, N. Perenne, and C. Talandier (2014), Dynamical contribution to sea surface salinity variations in the eastern Gulf of Guinea based on numerical modeling, *Clim. Dyn*., 43(11), 3105-3122, doi:10.1007/s00382-014-2195-4.

Bonjean, F., and G. S. E. Lagerloef (2002), Diagnostic model and analysis of the surface currents in the tropical Pacific Ocean, *J. Phys. Oceanogr., 32(10),* 2938–2954, doi: 10.1175/1520-0485(2002)032<2938: DMAATOT>2.0.CO; 2.

Bourlès, B., et al. (2008), The PIRATA program: History, accomplishments, and future directions, *Bull. Am. Meteorol. Soc*., 89(8), 1111-1125, doi:10.1175/2008BAMS2462.1.

Boutin, J. et al. (2016), Sattelite and In Situ salinity Understanding Near-Surface Stratification and Subfootprint Variability, *BAMS*, 1391-1407, DOI:10.1175/BAMS-D-15-00032.1.

Burmeister, K., P. Brandt, and J. F. Lubbecke (2016), Revisiting the cause of the eastern equatorial Atlantic cold event in 2009, *J. Geophys. Res*. Oceans, 121, 4777-4789; doi: 10.1002/2016JC011719.

Camara, I., N. Kolodziejczyk, J. Mignot, A. Lazar, and A. T.Gaye (2015), On the seasonal variations of salinity of the tropical Atlantic mixed layer, *J. Geophys. Res. Oceans*, 120, 4441-4462, doi: 10.1002/2015JC010865.

Caniaux, G., H. Giordani, J.–L. Redelsperger, F. Guichard, E. Key, and M. Wade (2011), Coupling between the Atlantic cold tongue and the West African monsoon in boreal spring and summer, *J. Geophys. Res.*, 116, C04003, doi: 10.1029/2010JC006570.

Chang, P., T. Yamagata, P. Schope, S. K. Behera, J. Carton, W. S. Kessler, G. Meyers, T. Qu, F. Schott, S. Shetye, and S. P. Xie (2005), Climate fluctuations of tropical coupled systems-The Role of Ocean Dynamics, *J. Clim*- special section, vol19.

Conkright, M.E., et al (2002), World Ocean Atlas 2001: Objective Analyses, Data Statistics, and figures, CD-ROM Documentation. *National Oceanographic Data Center*, Sliver Spring, MD, 17 pp,

Da-Allada, C. Y., G. Alory., Y. du Penhoat., E. Kestenare, F. Durand., and N. M. Hounkonnou (2013), Seasonal mixed-layer salinity balance in the Tropical Atlantic Ocean: Mean sate and seasonal cycle, *J. Geophys. Res. Oceans*, 118, doi: 10.1029/2012JC008357.

Da-Allada, C. Y., G. Alory., Y. du Penhoat, J. Jouanno, N. M. Hounkonnou and E. Kestenare (2014a), Causes for the Recent Increase in Sea Surface Salinity in the north-eastern Gulf of Guinea, *African Journal of Marine Science*, 36:2, 197-205, doi:10.2989/1814232X.2014.927398.

Da-Allada, C. Y., Y. du Penhoat, J. Jouanno, G. Alory, and N. M. Hounkonnou (2014b), Modeled mixed-layer salinity balance in the Gulf of Guinea: Seasonal and interannual variability, *Ocean Dyn*., 64(12), 1783-1802, doi: 10.1007/s10236-014-0775-9.

Da-Allada, C. Y., F. Gaillard and N. Kolodziejczyk (2015), Mixed-layer salinity budget in the tropical Indian Ocean: seasonal cycle based only from observations, *Ocean Dyn.,* 65(6), 845-857, doi: 10.1007/s10236-015-0837-7.

Dai, A., and K. Trenberth (2002), Estimates of freshwater discharge from continents: latitudinal and seasonal variations, *J. Hydrometeor*, 3: 660-687.

de Boyer Montégut C., G. Madec, A. S. Fischer, A. Lazar, and D. Ludicone (2004), Mixed layer depth over the global ocean: An examination of profile data and a profile-based climatology, *J. Geophys Res-Oceans,* 109, C12003, doi:10.1029/2004JC002378.

Dee, D. P., et al (2011), The ERA-Interim reanalysis: configuration and performance of the data assimilation system. *Q. J. R. Meteorol. Soc. 137*: 553–597. doi:10.1002/qj.828.

Dong, S., S. L. Garzoli, and M. Baringer (2009), An assessment of the seasonal mixed layer salinity budget in the Southern Ocean, *J. Geophys. Res.*, *114*, C12001, doi: 10.1029/2008JC005258.

Durack, P. J., and S. E. Wijffels (2010), Fifty-year trends in global ocean salinities and their relationship to broad-scale warming, *J. Clim.* 23(16), 4342-4362, doi: 10.1175/2010JCLI3377.1.

Dussin, R., B. Barnier and L. Brodeau, (2014), The making of Drakkar forcing set DFS5. *DRAKKAR/MyOcean Report* 05-10-14.

Foltz, G. R., S. A. Grodsky, J. A. Carton and M. J. McPhaden (2004), Seasonal salt budget of the northwestern tropical Atlantic Ocean along 38 °W, *J. Geophys. Res.*, 109, C03052, doi: 10.1029/2003JC002111.

Foltz, G. R. and M. J. McPhaden (2008), Seasonal mixed layer salinity balance of the tropical North Atlantic Ocean, *J. Geophys. Res.*, *113*, C02013, doi: 10.1029/2007JC004178.

Gaillard, F., T. Reynaud, V. Thierry, N. Kolodziejczyk, and K. von Schuckmann (2016), In-situ based reanalysis of the global ocean temperature and salinity with ISAS: variability of the heat content and steric height, *J. Clim.*, 29(4), 1305-1323, http://doi.org/10.1175/JCLI-D-15-0028.1.

Giordani, H. and G. Caniaux (2011), Diagnosing vertical motion in the Equatorial Atlantic, Ocean Dyn., 61:1995-2019, doi: 10. 1007/s10236-011-0467-7.

Gouriou, Y. and G. Reverdin (1992), Isopycnal and diapycnal circulation of the upper equatorial Atlantic Ocean in 1983-1984, *J. Geophys. Res*. 97: 3543-3572.

Hastenrath, S., and P. Lamb (1978), On the dynamics and climatology of surface flow over the equatorial oceans, *Tellus*, 30:436-448, doi: 10.1111/j.2153-3490.1978.tb00859.x.

Helm, K. P., N. L. Bindoff, and J. A. Church (2010), Changes in the global hydrological-cycle inferred from ocean salinity, *Geophys. Res. Lett.*, 37, L16701, doi: 10.1029/2010GL044222.

Hernandez, O., J. Boutin, N. Kolodziejczyk, G. Reverdin, N. Martin, F. Gaillard, N. Reul, and J.L. Vergely (2014), SMOS salinity in the subtropical north Atlantic salinity maximum:1. Comparison with Aquarius and in situ salinity, *J. Geophys Res. Oceans*, 119, 8878-8896, doi: 10.1002/2013JC009610.

Hernandez, O., J. Jouanno, and F. Durand (2016), Do the Amazon and Orinoco freshwater plumes really matter for hurricane-induced ocean surface cooling?, *J. Geophys. Res. Oceans*, 121, doi: 10.1002/2015JC011021.

Hosoda, S., T. Suga, N. Shikama, and K. Mizuno (2009), Global surface layer salinity change detected by Argo and its implication for hydrological cycle intensification, *J. Oceanogr.*, 65, 579-586.

Hummels, R., M. Dengler, and B. Bourlès (2013), Seasonal and regional variability of upper ocean diapycnal heat flux in the Atlantic cold tongue, *Prog. Oceanogr.*, 111, 52-74, doi:10.1016/j.pocean.2012.11.001.

Johns, W.E., P. Brandt, B. Bourlès, A. Tantet, A. Papapostolou, and A. Houk (2014), Zonal structure and seasonal variability of the Atlantic equatorial undercurrent, *Clim. Dyn.*, 1-22, doi:10.1007/s00382-014-2136-2

Jouanno, J., F. Marin, Y. du Penhoat, J. Sheinbaum, and J. M. Molines (2011), Seasonal heat balance in the upper 100 m of the equatorial Atlantic Ocean, *J. Geophys. Res., 116*, C09003, doi: 10.1029/2010JC006912.

Kolodziejczyk, N., B. Bourlès, F. Marin, J. Grelet and R. Chuchla (2009), Seasonal variability of the equatorial Undercurrent at 10°W as inferred from recent in situ observations, *J. Geophys. Res*. 114:C06014, doi: 10. 1029/2008JC004976.

Kolodziejczyk, N., F. Marin, B. Bourlès, Y. Gouriou, and H. Berger (2014), Seasonal variability of the equatorial undercurrent termination and associated salinity maximum in the Gulf of Guinea, *Clim. Dyn.*, 43: 3025-3046, doi:10.1007/s00382-014-2107-7.

Kummerow, C., W. Barnes, T. Kozu, J. Shiue, and J. Simpson (1998), The Tropical Rainfall Measuring Mission (TRMM) sensor package, *J. Atmos. Oceanic Technol*., 15, 809-817.

Lagerlof, G. S. E., G. T. Mitchum, R. B. Lukas and P. P. Niiler (1999), Tropical Pacific near-surface currents estimated from altimeter, wind, and drifter data, *J. Geophys. Res*., 104 (C10), 23, 313-23, 326.

Lagerlof, G.S.E (2012), Satellite mission monitors ocean surface salinity, *Eos Trans. AGU,* 93(25), 233-240, doi: 10.1029/2012EO250001.

Large, W., and S. Yeager (2004), Diurnal to decadal global forcing for ocean sea ice models: The data sets and flux climatologies. Rep. NCAR/TN-460+STR, *Natl. Cent. for Atmos. Res.*, Boulder, Colorado.

Lee, T., G. Lagerloef, M. M. Gierach, H.-Y. Kao, S. Yueh, and K. Dohan (2012), Aquarius reveals salinity structure of tropical instability waves, *Geophys. Res. Lett.*, 39, L12610, doi: 10.1029/2012GL052232.

Lee, T., G. Lagerloef, H.Y. Kao, M. J. Mcphaden, J. Willis, and M.M. Gierach (2014), The influence of salinity on tropical Atlantic instability waves, *J. Geophys. Res. Oceans*, 119, 8375-8394, doi: 10.1002/2014JC010100.

Lu, Z., L. Cheng, J. Zhu, and R. Lin (2016), The complementary role of SMOS sea surface salinity observations for estimating global ocean salinity state, *J. Geophys. Res. Oceans*, 121, doi:10.1002/2015JC011480.

Lukas, R., and E. Lindstrom (1991), The mixed layer of the western equatorial Pacific Ocean, *J. Geophys. Res.*, *96*, suppl., 3343–3357.

Madec, G. (2014), “NEMO ocean engine” (Draft edition r5171). Note du Pôle de modélisation, Institut Pierre-Simon Lapalce (IPSL), France, No 27 ISSN No 1288-1619.

Maes, C., and T. J. O’Kane (2014), Seasonal variations of the upper ocean salinity stratification in the Tropics, *J. Geophys. Res. Oceans*, 119, 1706-1722, doi: 10.1002/2013JC009366.

Marin, F., G. Caniaux, H. Giordani, B. Bourlès, Y. Gouriou, and E. Key (2009), Why were sea surface temperatures so different in the eastern equatorial Atlantic in June 2005 and 2006? *J. Phys. Oceanogr* 39:1416-1431

O’Kane, T. J., D. P. Monselesan, and C. Maes (2016), On the stability and spatiotemporal variance distribution of salinity in the upper ocean, *J. Geophys. Res. Oceans*, 121, 4128–4148, doi: 10.1002/2015JC011523.

Pailler, K., B. Bourlès, and Y. Gouriou (1999), The barrier layer in the western tropical Atlantic Ocean, *Geophys. Res. Lett.*, 38. Doi:10.1029/2011gl1046757.

Peter A-C., M. Le Hénaff, Y. du Penhoat, C. E. Menkes, F. Marin, J. Vialard, G. Caniaux, and A. Lazar (2006), A model study of the seasonal mixed-layer heat budget in the equatorial Atlantic, *J. Geophys. Res.*, 111: C06014, doi: 10. 1029/2005JC003157.

Perez, R. C., V. Hormann, R. Lumpkin, P. Brandt, W. E. Johns, F. Hernandez, C. Schmid, and B. Bourlès (2014), Mean meridional currents in the central and eastern equatorial Atlantic, *Clim. Dyn*, 43:2943-2962, doi:10,1007/s00382-013-1968-5.

Philander, S. G. H., and R. C. Pacanowski (1981), The oceanic response to cross-equatorial winds (with application to coastal upwelling in low latitudes), *Tellus*, 33(2), 201-210, doi: 10.1111/j.2153-3490.1981.tb01744.x.

Picaut, J. (1983), Propagation of the seasonal upwelling in the eastern equatorial Atlantic, *J. Phys. Oceanogr.*, vol13, n°1, 18-37.

Qu, T., S. Gao, and I. Fukumori (2011), What governs the North Atlantic salinity maximum in a global GCM? *Geophys. Res. Lett.*, 38.doi:10.1029/2011gl046757.

Reffrary, G., R. Bourdalle-Badie, and C. Calone (2015), Modelling turbulent vertical mixing sensitivity using a 1-D version of NEMO, *Geosci. Model Dev.*, 8, 69-86, doi: 10.5194/gmd-8-69-2015.

Ren, L., E. Hackert, P. Arkin, and A. J. Busalacchi (2014), estimating the global oceanic net freshwater flux from Argo and comparing it with satellite-based freshwater flux products, *J. Geophys. Res. Oceans*, 119, doi: 10.1002/2013JC009620.

Reul, N., and J. Tenerelli (2011), SMOS level 3 SSS research products: Product validation document reprocessed year 2010, Tech. Doc. CATDS-CECOS-L3-VALDOC, Inst.fr.de Rech. Pour l'Exploit. de la Mer, Brest, France. [Available at http://www.ifremer.fr/naiad/salinityremotesensing.ifremer.fr/CATDS_CECOS_SMOS_Level3Products_Validation.pdf.]

Reul, N., J. Tenerelli, J. Boutin, B. Chapron, F. Paul, E. Brion, F. Gaillard, and O. Archer (2012), Overview of the first SMOS sea surface salinity products, *IEEE Trans. Geosci. Remote. Sen.*, 50(5), 1636-1647, doi: 10.1109/TGRS.2012.21884081.

Reul, N., Y. Quilfen, B. Chapron, S. Fournier, V. Kudryavtsev, and R. Sabia (2014a), Multisensor observations of the Amazon-Orinoco River plume interactions with hurricanes, *J. Geophys. Res. Oceans*, 119, doi: 10.1002/2014JC010107.

Reul, N., S. Fournier, J. Boutin, O. Hernandez, C. Maes, B. Chapron, G. Alory, Y. Quilfen, J. Tenerelli, S. Morisset, Y. Kerr, S. Mecklenburg, and S. Delwart (2014b), Sea surface salinity observations from space with SMOS satellite: a new tool to better monitor the marine branch of the water cycle, *Surv. Geophys*, 35:681, 722.doi:10,1007/s10712-013-9244-0.

Rhein, M., M. Dengler, J. Sültenfuß, R. Hummels, S. Hüttl-Kabus, and B. Bourlès (2010), Upwelling and associated heat flux in the equatorial Atlantic inferred from Helium isotope disequilibrium, *J. Geophys. Res.*, 115, C08021, doi:10.1029/2009JC005772.

Schlundt, M., P. Brandt, M. Dengler, R. Hummels, T. Fischer, K. Bumke, G. Krahmann, and J. Karstensen (2014), Mixed layer heat and salinity budgets during the onset of the 2011 Atlantic cold tongue, *J. Geophys. Res. Oceans*, 119, doi: 10.1002/2014JC010021.

Sprintall, J., and M. Tomczak (1992), Evidence of the barrier layer in the surface layer of the tropics, *J. Geophys. Res., 97*, 7305– 7316.

Terray, L., L. Corre, S. Cravatte, T. Delcroix, G. Reverdin and A. Ribes (2012), Near-surface salinity as nature's rain gauge to detect human influence on the tropical water cycle, *J. Clim.* 25, 958-977, doi:10.1175/JCLI-D-10-05025.1.

Tzortzi, E., S. A. Josey, M. Srokosz and C. Gommenginger (2013), Tropical Atlantic Salinity variability: New insights from SMOS, *Geophys. Res. Lett.*, 40, 2143-2147, doi:10.1002/grl.50225.

Umlauf, L., and H. Burchard (2003), A generic length-scale equation for geophysical turbulence models. *J. Mar. Res*. 61(31), 235-265.

Wade, M., G. Caniaux, and Y. du Penhoat (2011), Variability of the mixed layer heat budget in the eastern equatorial Atlantic during 2005-2007 as inferred using Argo floats, *J. Geophys. Res.*, 116, C08006, doi: 10.1029/2010JC006683.

Waliser, D. E., and C. Gautier (1993), A satellite-derived climatology of the ITCZ, *J. Clim.*, 6:2162-2174.

Webster, P. J. (1994), The role of hydrological processes in ocean atmosphere interactions, *Rev. Geophys.*, 32, 427–476.

Yu, L. (2011), A global relationship between the ocean water cycle and near surface salinity, *J. Geophys. Res., 116*, C10025, doi: 10.1029/2010JC006937.

Figure Captions:

Figure 1. a) Satellite-SST distribution during July showing the spatial extend of the equatorial Atlantic Cold tongue (ACT) region. Contours represent 23, 24 and 25 °C isotherms. b) Seasonal evolution of the SSS (blue lines) and the SST (red lines) for the satellite observations (full lines) and the model (dashed lines) in the ACT (box marked in a). The seasonal cycle of the SSS and of the SST is computed for the 2010-2012 period. Units are °C (a, b) and PSS (b).

Figure 2. Seasonal salinity (PSS unit) evolution at (0°N-10°W) between 0 and 90 m depth computed for the 2010-2012 period: a) PIRATA mooring and b) model output. Dashed lines represent the 35.5 and 36 PSS isohalines. Note that a pronounced subsurface salinity maximum, associated with the EUC between 40 and 80 m is not fully captured by the PIRATA data due to sparse vertical sampling of salinity over the vertical due to mooring design or salinity sensor failures.

Figure 3. Same as Figure 2 but for temperature (°C). Contours represent the 20°C and 24°C isotherms.

Figure 4. Seasonal SSS budget for the ACT region computed for the 2010-2012 period. a) Observations (black) and model (red) salinity tendencies (lhs term of Eq.1) with the shaded areas indicating error estimates for the observed salinity tendency. b) The different contributions of the salinity equation (rhs terms of Eq.1) for the observations (full lines) and the model (dashed lines): surface freshwater flux (FLX in magenta), vertical processes (VPR in green), horizontal advection (HAD in blue) and lateral diffusion (LDF in light blue). The units are pss.month^{-1} for a) and b).

Figure 5. a) Horizontal salinity advection (HAD in dashed blue) contributions: zonal advection (XAD in black) and meridional advection (YAD in dashed lack). b) Vertical processes contributions to the SSS seasonal variability (VPR in dashed green): vertical salinity advection (ZAD in pink), vertical diffusion (ZDF in red) and the entrainment term (ENT in dashed black). All the terms are explained in Eq.1. The units are pss.month^{-1} for (a) and (b).

Figure 6. Seasonal evolution of model vertical profiles computed for the 2010-2012 period in the ACT box: a) vertical diffusion (ZDF in color shading; PSS.month^{-1}) and salinity (contours in black dashed line; PSS), b) log10 of the Richardson number (color shading) and turbulent salinity flux (TSF, contours in dashed line black; PSS.month^{-1}.m), c) square vertical shear of the zonal currents only (Shu^2 in color shading; in 10^{-4} s^{-2}) and TSF_{ZDF} (in dashed line black contours), and d) total square vertical shear (Sh^2 color shading; in 10^{-4} s^{-2}) and TSF_{ZDF} (in dashed line black contours). The depth of the isopycnals 24.7 and 26 kg m^{-3} are superimposed in blue dashed lines. The thick black lines are mixed-layer depth (MLD).

Figure 7. Seasonal evolution of model vertical profiles computed for the 2010-2012 period in the ACT: a) zonal current (U in color shading; m s^{-1}), b) horizontal velocity (color shading; m s^{-1},), c) the vertical salinity stratification on Brunt –Väisälä frequency ($N2_{(S)}$ in color shading; 10^{-4} s^{-2}), d) vertical velocity (W in color shading; 10^{-6} m s^{-1}) and e) wind stress (10^{-1} N.m^{-2}; red line is total, black line is zonal, dashed black line is meridional). The depth of the isopycnals 24.7 and 26 kg m^{-3} and salinity are superimposed in blue dashed lines and in black dashed line. The thick black lines are MLDs and the thick red line indicate the 20°C isotherm

Figure 8. Model seasonal profile in the ACT region between 0 and 90 m depth computed for the 2010-2012 period for: a) salinity (in PSS) and b) temperature (in °C). Black dashed lines indicate the 36 PSS isohaline and in b) the solid red line indicate the 20°C isotherm. Isopycnals 24.7 and 26 kg m^{-3} are superimposed in blue dashed lines for a) and b). The thick black lines indicate mixed-layer depth (MLD).

Figure 9. Time-latitude diagrams of the mean seasonal cycle computed for the 2010-2012 period in the EUC delimited by the 24.7-26 kg.m^{-3} isopycnals in the model between 17°W-0° and 3°N-3°S : a) salinity, contours represent the 36, 36.1 and 36.2 PSS isohalines; b) zonal current with contours interval of 0.2 m.s^{-1}; and c) the meridional current with contours interval of 0. 03 m.s^{-1}.

Figure 10. Longitude-time diagram of the mean seasonal cycle of the EUC salinity (in PSS; color shading) and currents (in cm.s^{-1} ; vectors) computed for the 2010-2012 period between isopycnals 24.7 and 26 kg m^{-3} at 1°N-3°S and between 40°W and 10°E. The dashed white lines at 17°W and 0°E indicate the western and eastern boundary of the ACT. Contours represent the 36, 36.1 and 36.2 isohalines.

Figure 11. The seasonal salinity budget within the σ=24.7–26 kg m^{-3} layer in the ACT computed for the 2010-2012 period. The ACT-averaged salinity budget is decomposed in the salt tendency (red), zonal salt advection (XSF in solid black), meridional salt advection (YSF in dashed black), vertical salt advection (ZSF in pink) and the turbulent salt (TSF in green). Unit is PSS.$month^{-1}$.

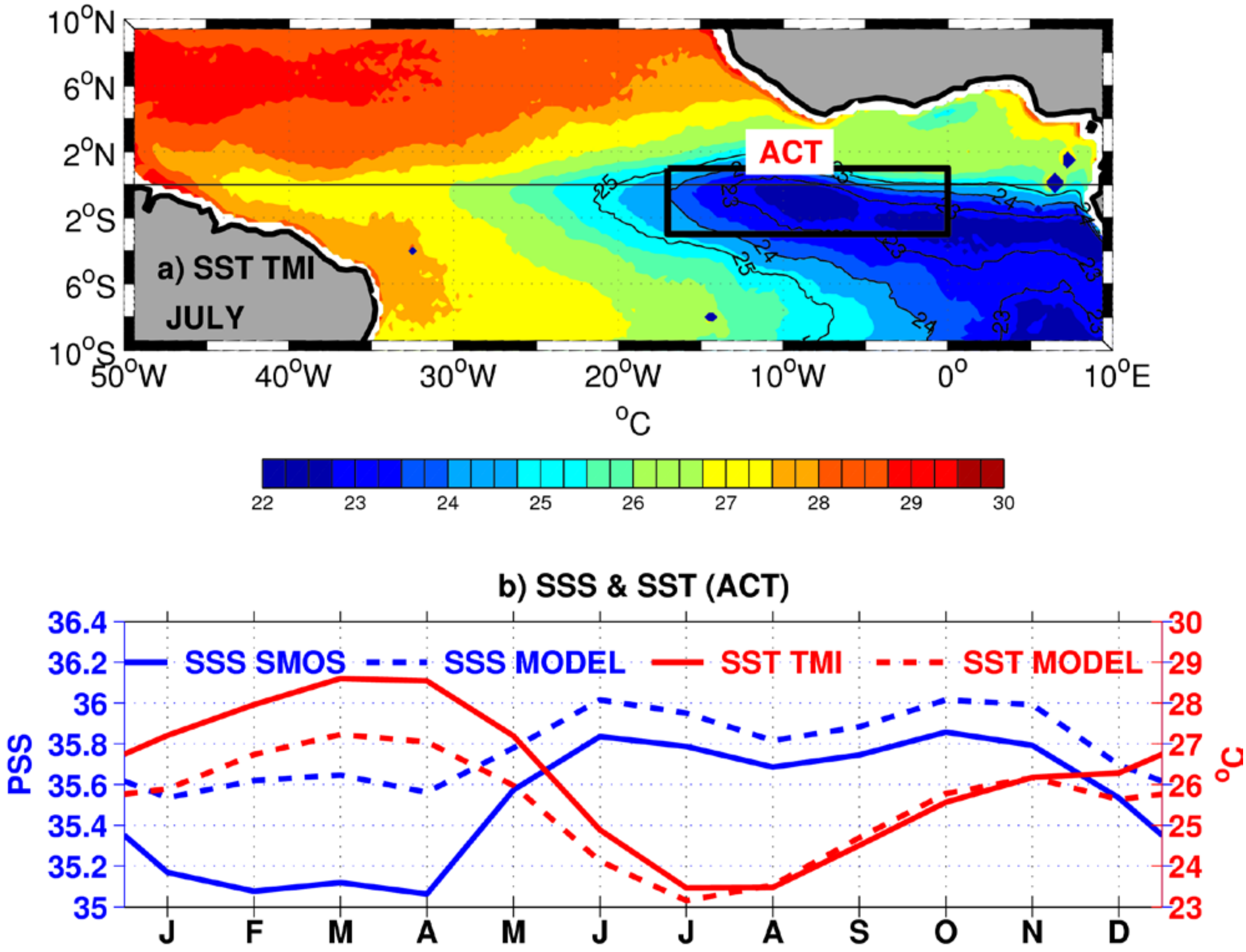

Figure 1. a) Satellite-SST distribution during July showing the spatial extend of the equatorial Atlantic Cold tongue (ACT) region. Contours represent 23, 24 and 25 °C isotherms. b) Seasonal evolution of the SSS (blue lines) and the SST (red lines) for the satellite observations (full lines) and the model (dashed lines) in the ACT (box marked in a). The seasonal cycle of the SSS and of the SST is computed for the 2010-2012 period. Units are °C (a, b) and PSS (b).

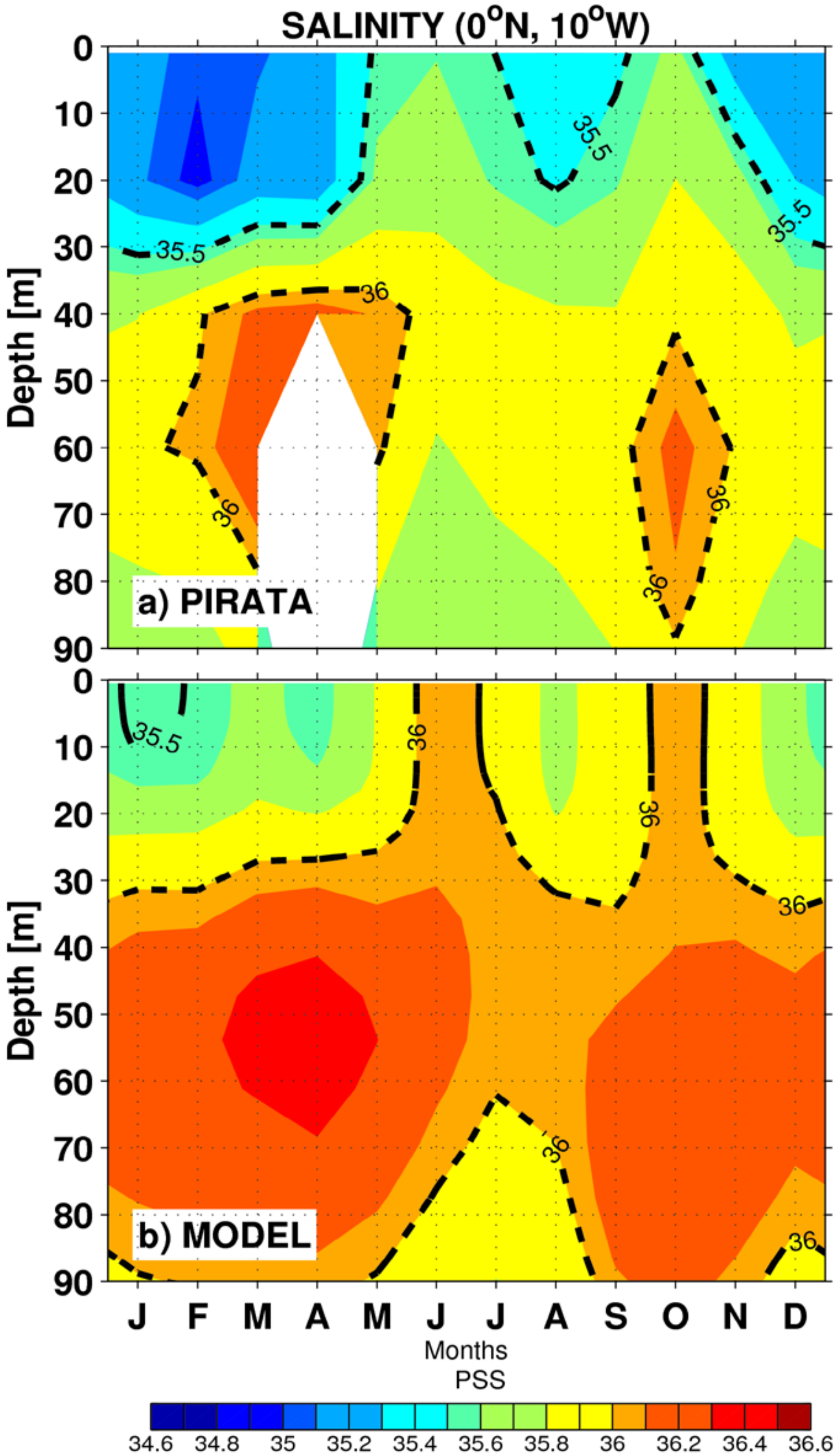

Figure 2. Seasonal salinity (PSS unit) evolution at (0°N-10°W) between 0 and 90 m depth computed for the 2010-2012 period: a) PIRATA mooring and b) model output. Dashed lines represent the 35.5 and 36 PSS isohalines. Note that a pronounced subsurface salinity

maximum, associated with the EUC between 40 and 80 m is not fully captured by the PIRATA data due to sparse vertical sampling of salinity over the vertical due to mooring design or salinity sensor failures.

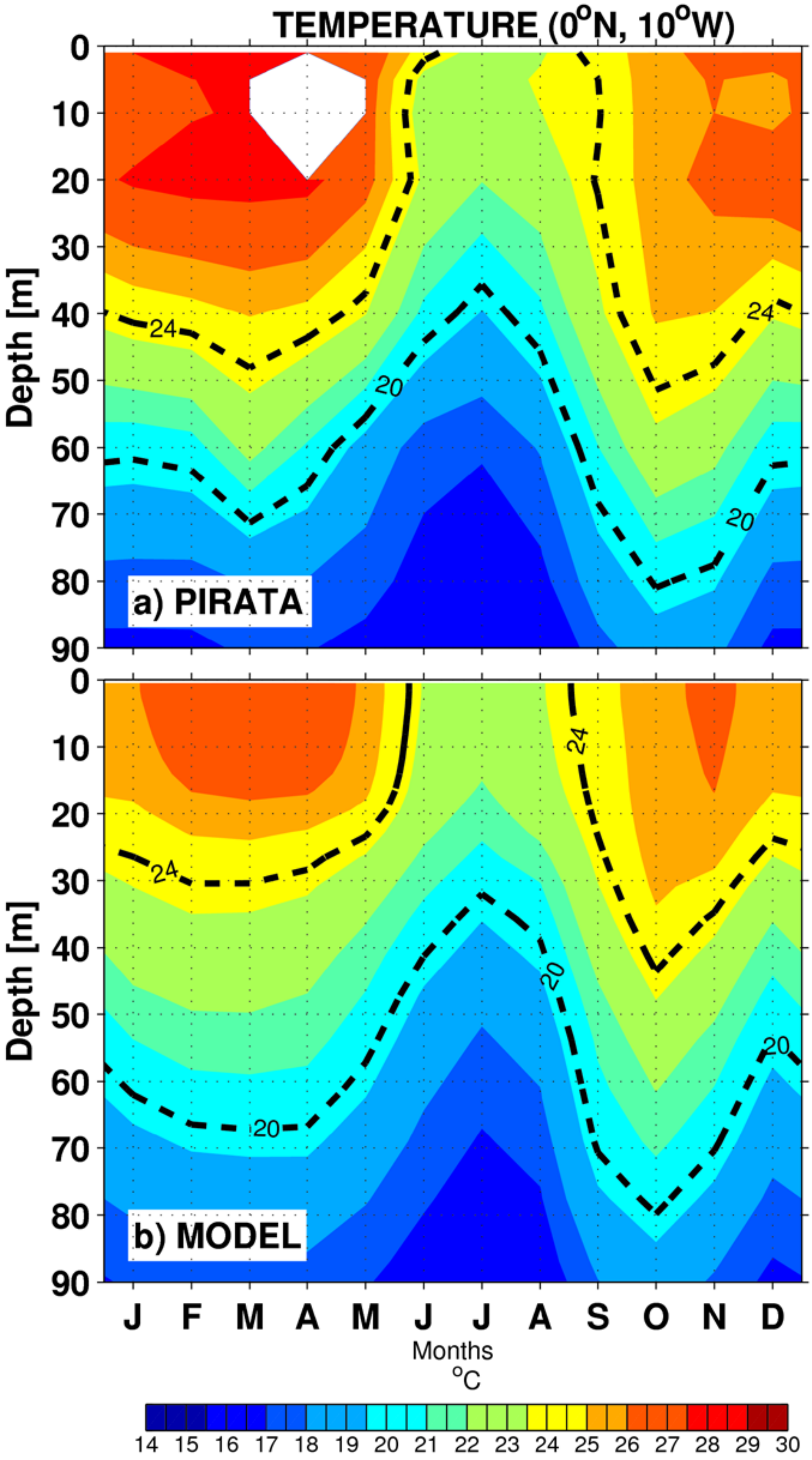

Figure 3. Same as Figure 2 but for temperature (°C). Contours represent the 20 °C and 24 °C isotherms.

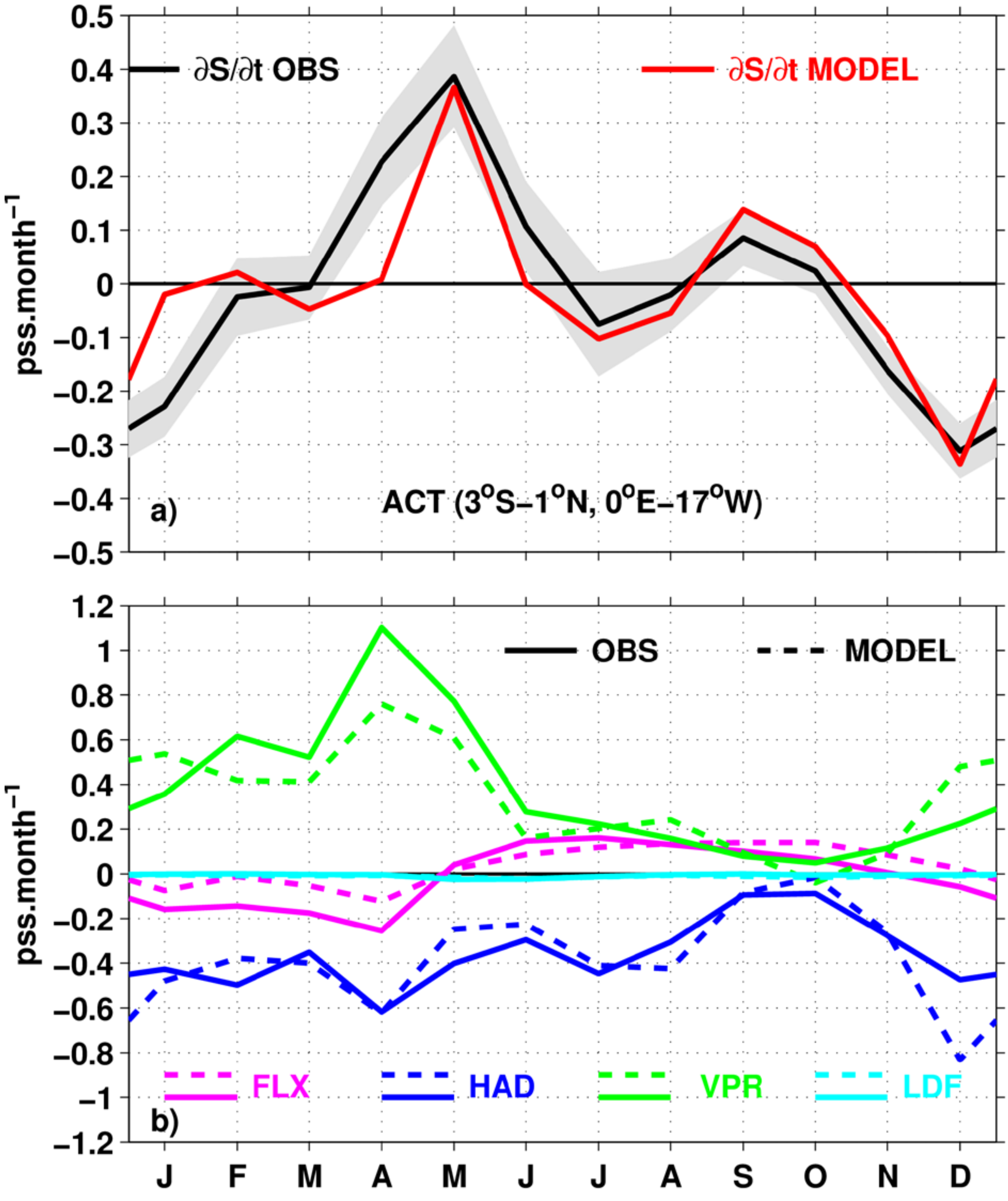

Figure 4. Seasonal SSS budget for the ACT region computed for the 2010-2012 period. a) Observations (black) and model (red) salinity tendencies (lhs term of Eq.1) with the shaded areas indicating error estimates for the observed salinity tendency. b) The different

contributions of the salinity equation (rhs terms of Eq.1) for the observations (full lines) and the model (dashed lines): surface freshwater flux (FLX in magenta), vertical processes (VPR in green), horizontal advection (HAD in blue) and lateral diffusion (LDF in light blue). The units are pss.month^{-1} for a) and b).

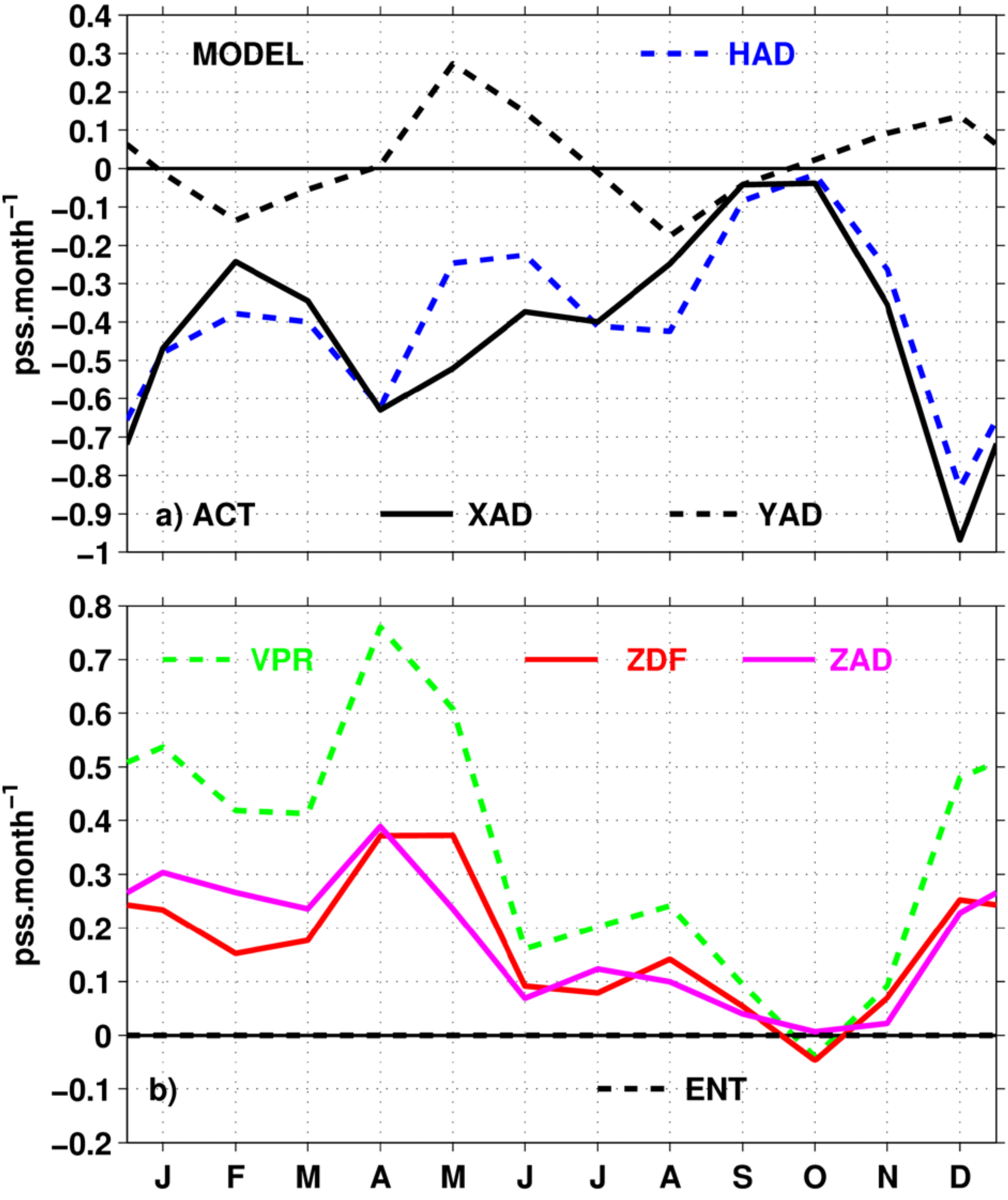

Figure 5. a) Horizontal salinity advection (HAD in dashed blue) contributions: zonal advection (XAD in black) and meridional advection (YAD in dashed lack). b) Vertical

processes contributions to the SSS seasonal variability (VPR in dashed green): vertical salinity advection (ZAD in pink), vertical diffusion (ZDF in red) and the entrainment term (ENT in dashed black). All the terms are explained in Eq.1. The units are pss.month^{-1} for (a) and (b).

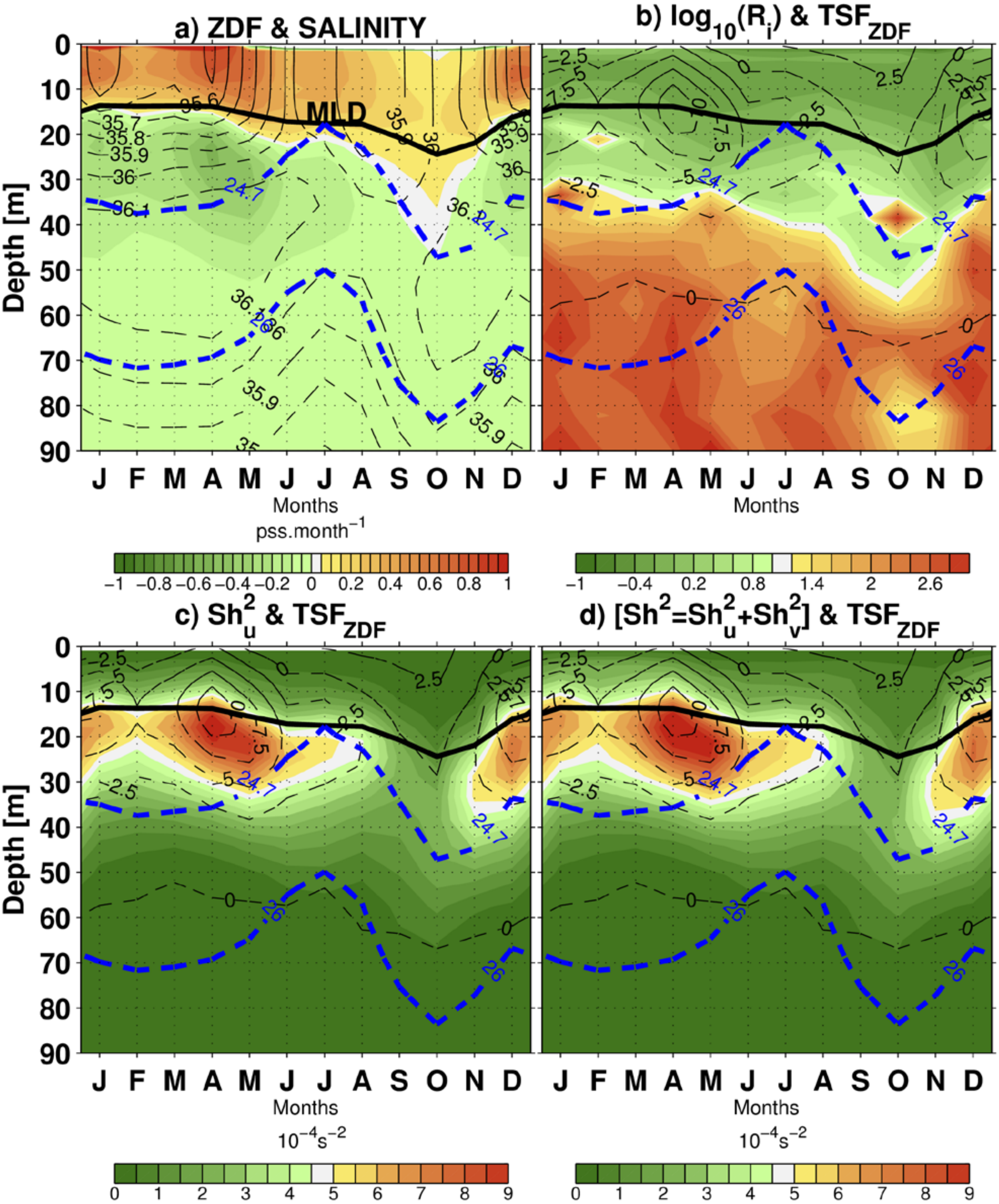

Figure 6. Seasonal evolution of model vertical profiles computed for the 2010-2012 period in the ACT box: a) vertical diffusion (ZDF in color shading; PSS.month^{-1}) and salinity (contours in black dashed line; PSS), b) log10 of the Richardson number (color shading) and turbulent

salinity flux (TSF, contours in dashed line black; PSS.month^{-1}.m), c) square vertical shear of the zonal currents only (Shu^2 in color shading; in 10^{-4} s^{-2}) and TSF_{ZDF} (in dashed line black contours), and d) total square vertical shear (Sh^2 color shading; in 10^{-4} s^{-2}) and TSF_{ZDF} (in dashed line black contours). The depth of the isopycnals 24.7 and 26 kg m^{-3} are superimposed in blue dashed lines. The thick black lines are mixed-layer depth (MLD).

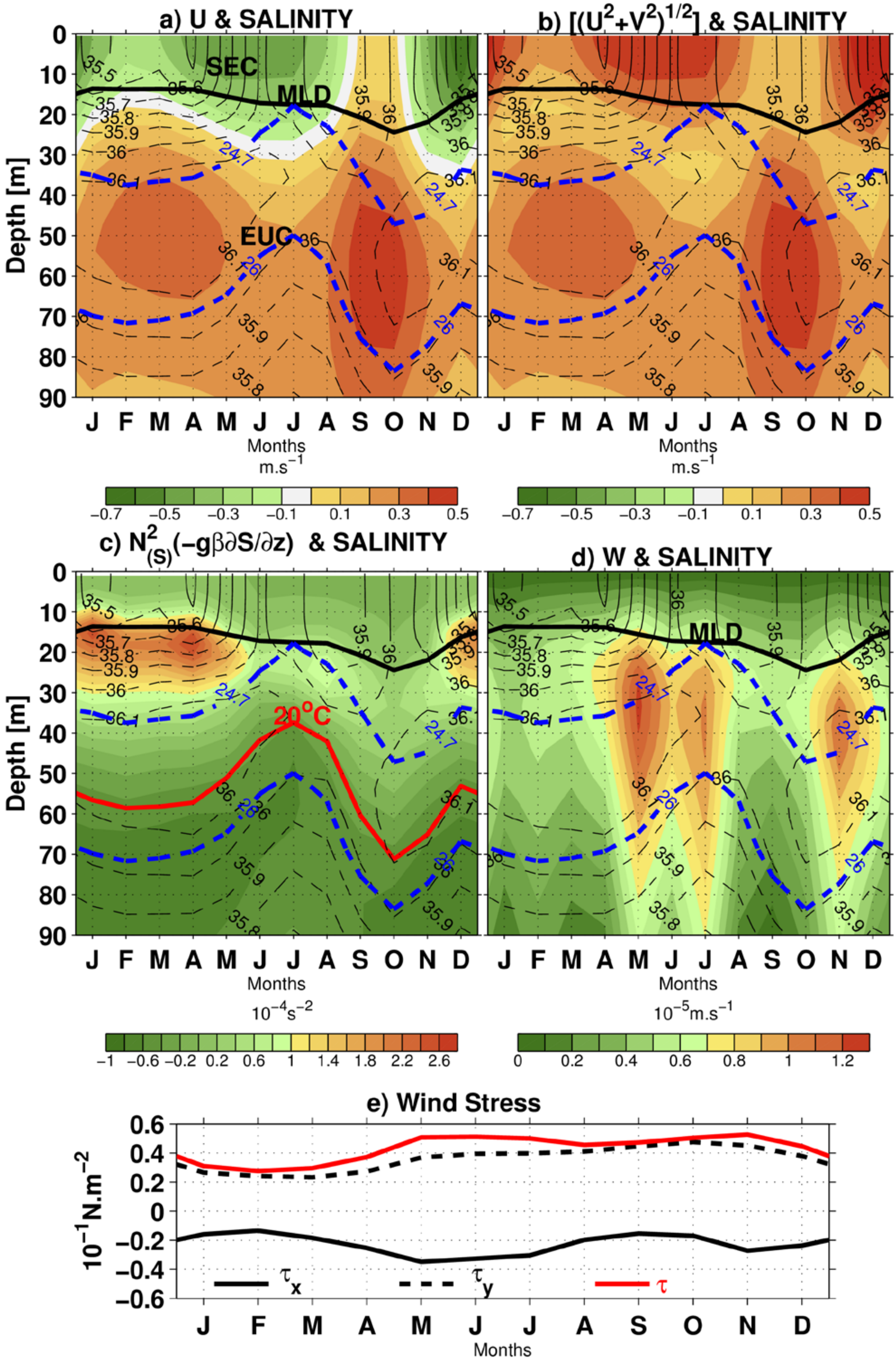
a) U & SALINITY
b) [(U²+V²)^1/2] & SALINITY
c) N²(S)(−gβ∂S/∂z) & SALINITY
d) W & SALINITY
e) Wind Stress
SEC
MLD
EUC
20°C
Depth [m]
Months
m.s⁻¹
10⁻⁴s⁻²
10⁻⁵m.s⁻¹
10⁻¹N.m⁻²
τx
τy
τ
J F M A M J J A S O N D

Figure 7. Seasonal evolution of model vertical profiles computed for the 2010-2012 period in the ACT: a) zonal current (U in color shading; m s^{-1}), b) horizontal velocity (color shading; m s^{-1},), c) the vertical salinity stratification on Brunt –Väisälä frequency ($N2_{(S)}$ in color shading; 10^{-4} s^{-2}), d) vertical velocity (W in color shading; 10^{-6} m s^{-1}) and e) wind stress (10^{-1} N.m^{-2}; red line is total, black line is zonal, dashed black line is meridional). The depth of the isopycnals 24.7 and 26 kg m^{-3} and salinity are superimposed in blue dashed lines and in black dashed line. The thick black lines are MLDs and the thick red line indicate the 20°C isotherm

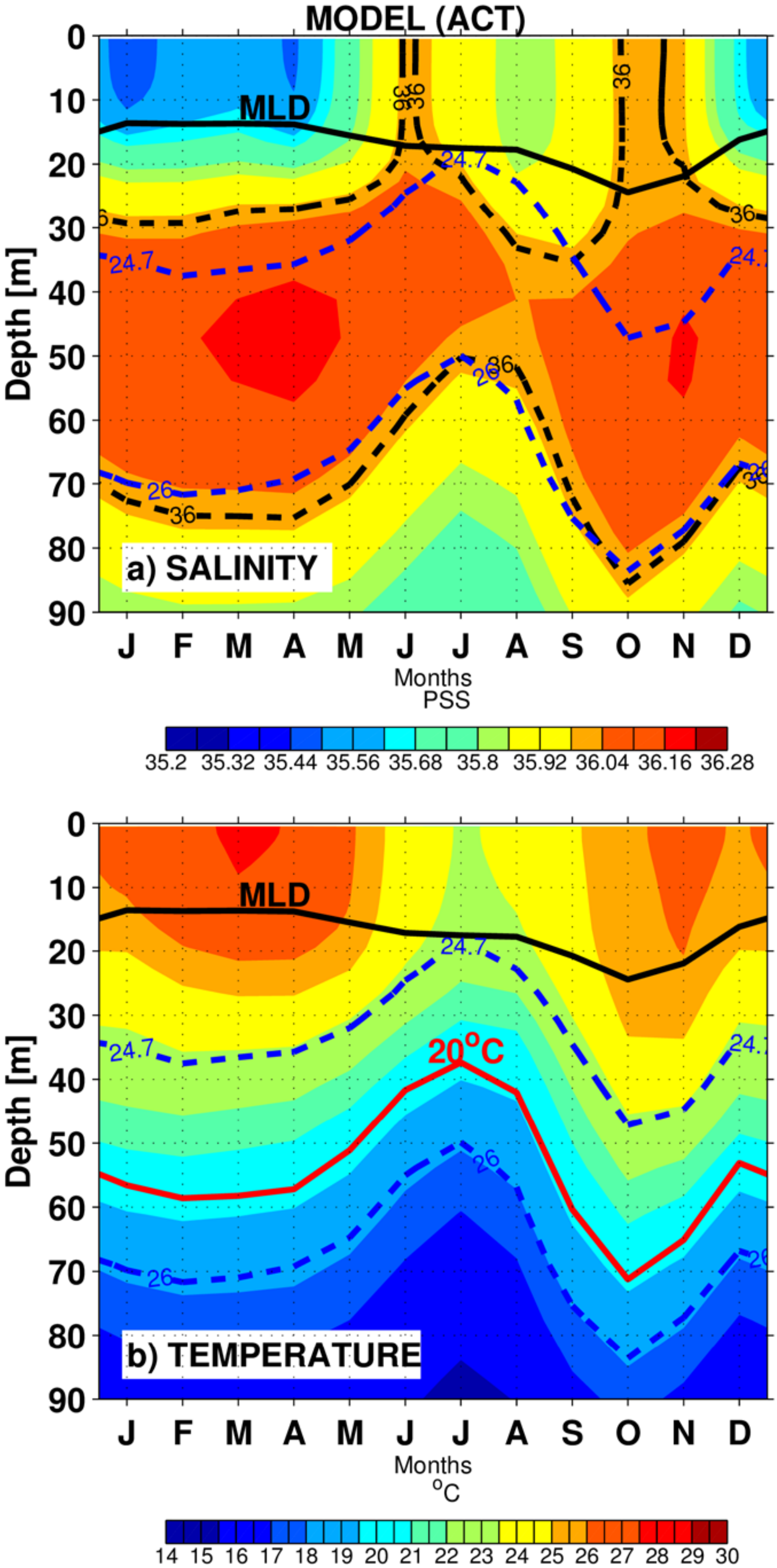
MODEL (ACT)
MLD
a) SALINITY
Depth [m]
Months
PSS
35.2 35.32 35.44 35.56 35.68 35.8 35.92 36.04 36.16 36.28
MLD
20°C
b) TEMPERATURE
Depth [m]
Months
°C
14 15 16 17 18 19 20 21 22 23 24 25 26 27 28 29 30

Figure 8. Model seasonal profile in the ACT region between 0 and 90 m depth computed for the 2010-2012 period for: a) salinity (in PSS) and b) temperature (in °C). Black dashed lines indicate the 36 PSS isohaline and in b) the solid red line indicate the 20°C isotherm. Isopycnals 24.7 and 26 kg.m^{-3} are superimposed in blue dashed lines for a) and b). The thick black lines indicate mixed-layer depth (MLD).

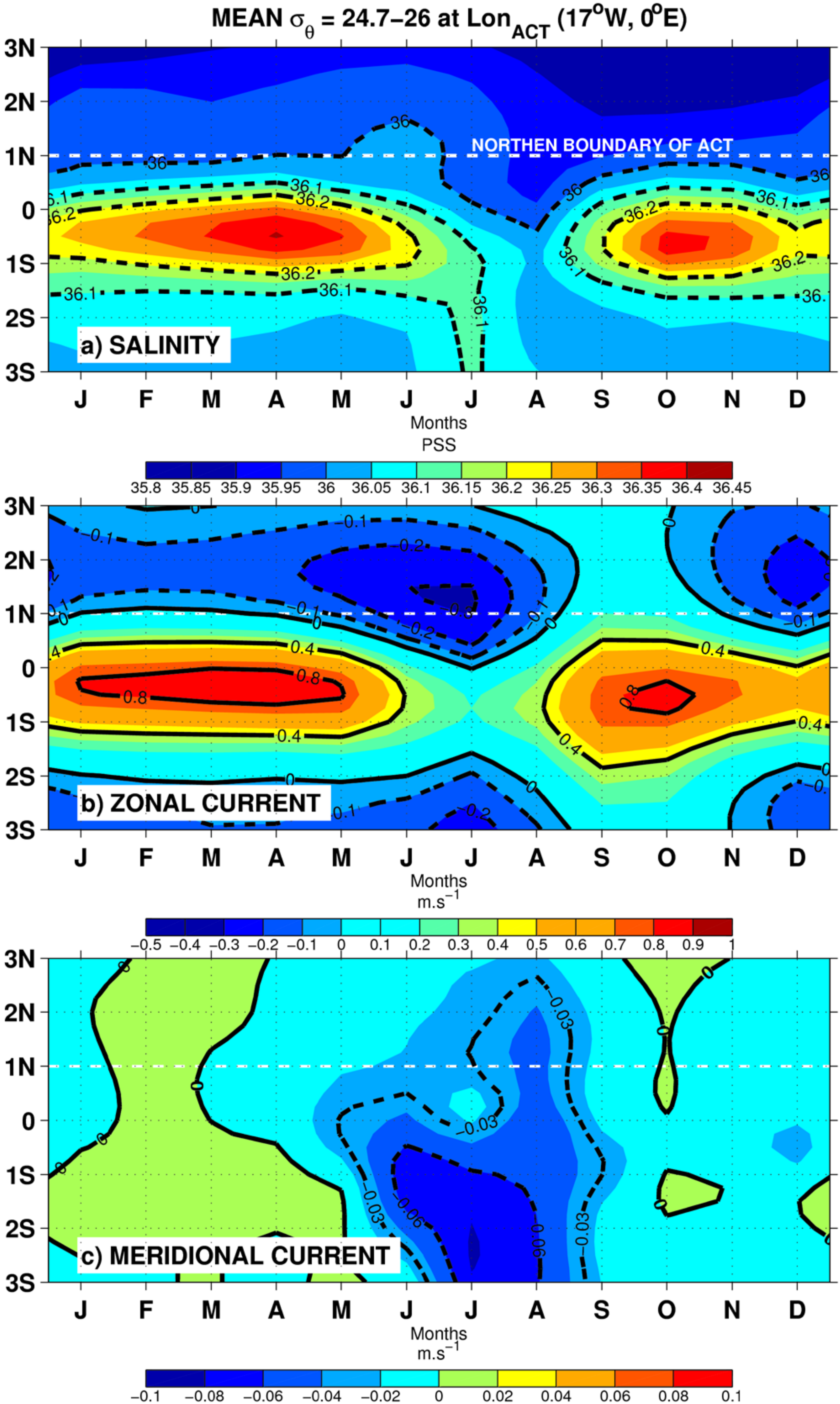
MEAN σ_θ = 24.7–26 at Lon$_{ACT}$ (17^{o}W, 0^{o}E)
NORTHEN BOUNDARY OF ACT
a) SALINITY
Months
PSS
b) ZONAL CURRENT
Months
m.s^{-1}
c) MERIDIONAL CURRENT
Months
m.s^{-1}

Figure 9. Time-latitude diagrams of the mean seasonal cycle computed for the 2010-2012 period in the EUC delimited by the 24.7-26 $kg.m^{-3}$ isopycnals in the model between 17°W-0° and 3°N-3°S : a) salinity, contours represent the 36, 36.1 and 36.2 PSS isohalines; b) zonal current with contours interval of 0.2 $m.s^{-1}$; and c) the meridional current with contours interval of 0. 03 $m.s^{-1}$.

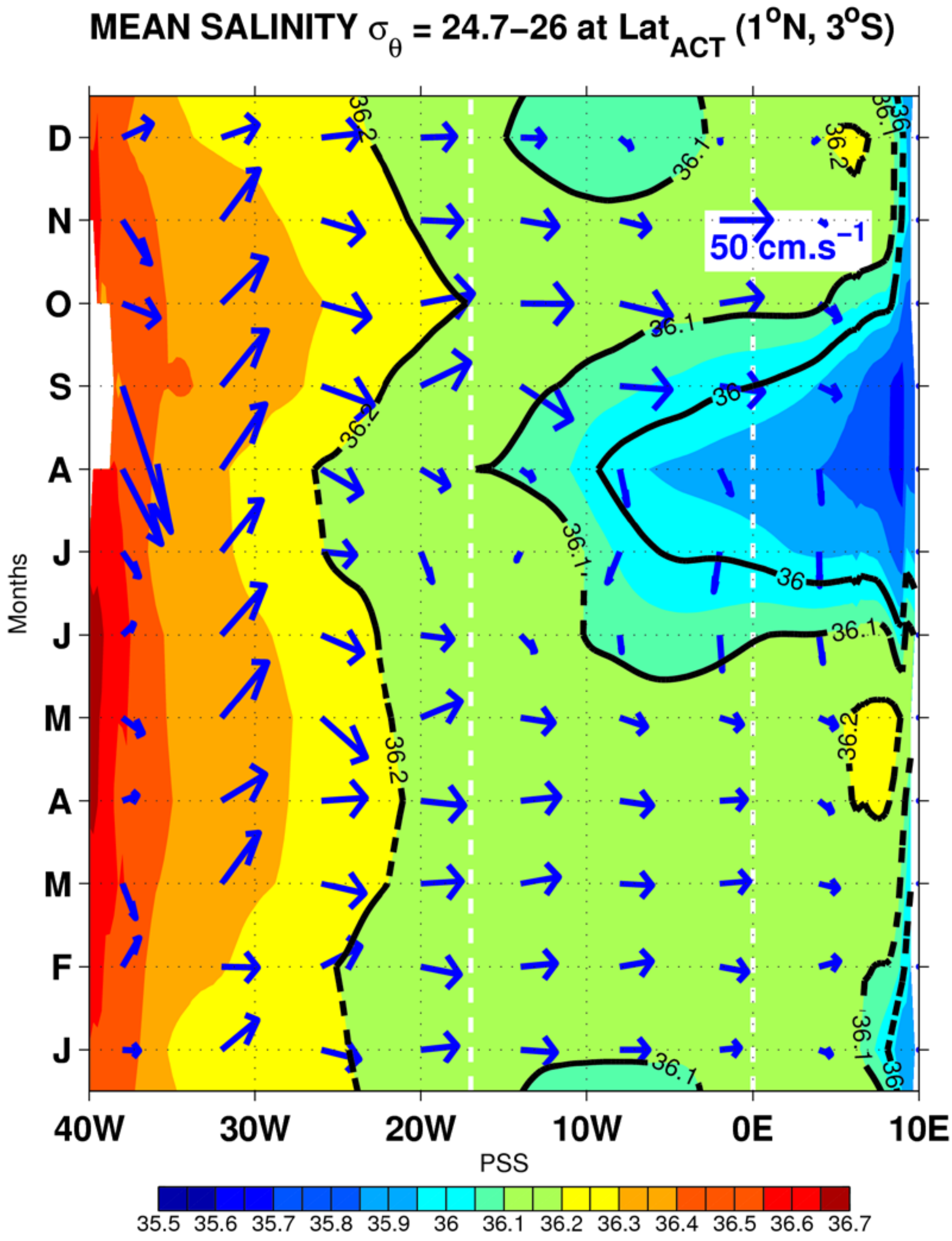

Figure 10. Longitude-time diagram of the mean seasonal cycle of the EUC salinity (in PSS; color shading) and currents (in cm.s^{-1} ; vectors) computed for the 2010-2012 period between isopycnals 24.7 and 26 kg m^{-3} at 1°N-3°S and between 40°W and 10°E. The dashed white

lines at 17°W and 0°E indicate the western and eastern boundary of the ACT. Contours represent the 36, 36.1 and 36.2 isohalines.

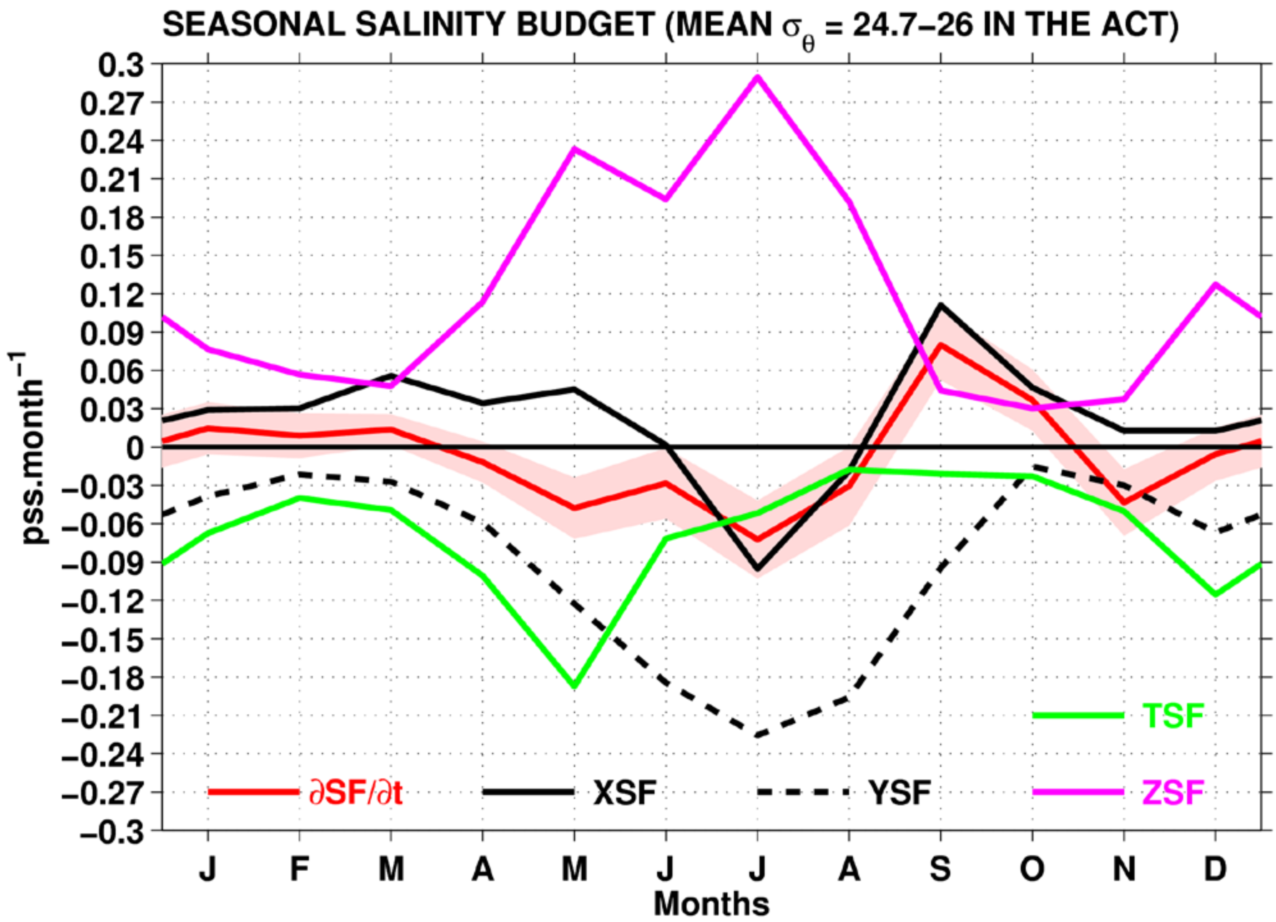

Figure 11. The seasonal salinity budget within the σ=24.7–26 kg.m^{-3} layer in the ACT computed for the 2010-2012 period. The ACT-averaged salinity budget is decomposed in the salt tendency (red), zonal salt advection (XSF in solid black), meridional salt advection (YSF in dashed black), vertical salt advection (ZSF in pink) and the turbulent salt (TSF in green). Unit is PSS.month^{-1}.